The American Journal of Pathology, Vol. 176, No. 2, February 2010

DOI: 10.2353/ajpath.2010.090744

Stem Cells, Tissue Engineering and Hematopoietic Elements

Blockade of Autoantibody-Initiated Tissue Damage by Using Recombinant Fab Antibody Fragments against Pathogenic Autoantigen

Gang Wang,*† Hideyuki Ujiie,* Akihiko Shibaki,* Wataru Nishie,* Yasuki Tateishi,* Kazuhiro Kikuchi,* Qiang Li,* James R. McMillan,*† Hiroshi Morioka,‡ Daisuke Sawamura,* Hideki Nakamura,* and Hiroshi Shimizu*

From the Department of Dermatology, Hokkaido University Graduate School of Medicine, the Creative Research Initiative Sousei,† and the Faculty of Pharmaceutical Sciences,‡ Hokkaido University, Sapporo, Japan*

Activation of the complement cascade via the classical pathway is required for the development of tissue injury in many autoantibody-mediated diseases. It therefore makes sense to block the pathological action of autoantibodies by preventing complement activation through inhibition of autoantibody binding to the corresponding pathogenic autoantigen using targeted Fab antibody fragments. To achieve this, we use bullous pemphigoid (BP) as an example of a typical autoimmune disease. Recombinant Fabs against the non-collagenous 16th-A domain of type XVII collagen, the main pathogenic epitope for autoantibodies in BP, were generated from antibody repertoires of BP patients by phage display. Two Fabs, Fab-B4 and Fab-19, showed marked ability to inhibit the binding of BP autoantibodies and subsequent complement activation *in vitro*. In the *in vivo* experiments using type XVII collagen humanized BP model mice, these Fabs protected mice against BP autoantibody-induced blistering disease. Thus, the blocking of pathogenic epitopes using engineered Fabs appears to demonstrate efficacy and may lead to disease-specific treatments for antibody-mediated autoimmune diseases. *(Am J Pathol 2010, 176:914–925; DOI: 10.2353/ajpath.2010.090744)*

Autoimmune diseases are a major cause of morbidity and mortality in humans, affecting approximately 5% of the general population.[1] In recent years, significant advances have been made in our understanding of autoimmune disease pathomechanisms, especially the roles of autoantibodies, complement system, and autoresponsive T cells. For many autoimmune diseases such as systemic lupus erythematosus, rheumatoid arthritis, anti-phospholipid syndrome (APS), and bullous pemphigoid (BP), complement activation is increasingly recognized as critical to tissue injury.[2–6] Studies of APS and BP, for example, showed that the classical pathway of complement activation is required for the development of tissue injury, although alternative pathways may also be involved.[4,7–9]

BP is the most common autoimmune blistering skin disease. Autoantibodies against collagen XVII (COL17) bind to dermal–epidermal junction (DEJ) components and activate the complement system that mediates a series of inflammatory events including dermal mast cell degranulation and generation of eosinophil-rich infiltrates, resulting in skin blister formation.[10–12] APS is a condition characterized by recurrent miscarriage and thrombosis formation in the presence of anti-phospholipid autoantibodies, and a therapy has been proven effective to prevent the fetal loss by using heparin to inhibit anti-phospholipid antibody–induced complement activation.[7,13,14] In both BP and APS, $F(ab')_2$ fragments from the pathogenic autoantibodies, which lack the Fc portion necessary to activate the complement pathway, fail to initiate the disease.[4,7] This suggests that preventing complement activation by blocking the binding of autoantibodies to the corresponding antigens can be a viable novel therapeutic strategy for treating these diseases.

Supported by a grant-in-aid from the Program for Promotion of Fundamental Studies in Health Sciences of the National Institute of Biomedical Innovation (NIBIO; to H.S.).

G.W. and H.U. contributed equally to this work. A.S. and H.S. contributed equally to the direction of this study.

Accepted for publication October 7, 2009.

Supplemental material for this article can be found on *http://ajp.amjpathol.org*.

Address reprint requests to Dr. Akihiko Shibaki or Dr. Hiroshi Shimizu, Department of Dermatology, Hokkaido University Graduate School of Medicine, N15 W7, Sapporo, 060-8638 Japan. E-mail: ashibaki@med.hokudai.ac.jp or shimizu@med.hokudai.ac.jp.

Table 1. PCR Primers for the Amplification of Human Antibody Gene Repertoires

Primers for κ	
HK5	5′-GAMATYGAGCTCACSCAGTCTCCA-3′ (Sac I)
HK3	5′-GCGCCGTCTAGAACTAACACTCTCCCCTGTTGAAGCTCTTTGTGACGGGCAAG-3′ (Xba I)
Primers for λ	
HL5	5′-CASTYTGAGCTCACKCARCCGCCCTC-3′ (Sac I)
HL3	5′-GAGGGATCTAGAATTATGAACATTCTGTAGG-3′ (Xba I)
Primers for Fd	
H135	5′-CAGGTGCAGCTGGTGSAGTCTGG-3′
H2	5′-CAGGTCAACTTGAAGGAGTCTGG-3′
H4	5′-CAGGTGCAGCTGCAGGAGTCGGG-3′
VH5	5′-CAGGTGCAGCTCGAGSAGTCTGG-3′ (Xho I)
HG3	5′-GCATGTACTAGTTTTGTCACAAGA-3′ (Spe I)

To allow for sequence variability, representative choices of wobble nucleotides were included in the primers (M = A/C, K = G/T, R = A/G, S = C/G, Y = C/T). Fd fragments of human IgG were amplified in a two-step procedure. First, antisense primers H135, H2, and H4 were combined with HG3 for the amplification of heavy chain genes from human VH1–VH5 families and the *Spe* I site was introduced. In the second step, antisense primer VH5 was combined with HG3 to reamplify the heavy chain genes and introduce the *Xho* I site. Underlined sequences are restriction sites for the enzymes indicated in parenthesis.

The purpose of this study is to provide a proof of concept for this new strategy of treating antibody-mediated autoimmune disorders by using recombinant Fabs to block complement activation induced by pathogenic autoantibodies. Toward this end, we use BP as an example of a typical autoimmune disease. Our group has recently established a BP mouse model using a newly constructed COL17 humanized mouse.[3] Here we report our success in developing Fabs against the noncollagenous 16th-A domain (NC16A) of COL17, the main pathogenic epitope of BP autoantibodies,[15] for the blockade of autoantibody-initiated BP disease.

Materials and Methods

Construction of Phage Antibody Libraries

We constructed two individual Fab phage libraries from mononuclear cells isolated from two patients with active BP. The diagnosis of BP was made by the typical clinical and histological manifestations as well as by laboratory data including anti-COL17 ELISA and indirect immunofluorescence (IIF). Phagemid expression vector p3MH, a gift from Dr. Yan Wang (Central Lab of Navy General Hospital, Beijing, China), was derived from pCOMB3H (Scripps Research Institute, La Jolla, CA) by adding 9E10/c-*myc* epitope for detection and a hexahistidine tag for column purification at the 3′ end of Fd.[16] Using previously described methods and a set of PCR primers (Table 1),[17–19] antibody genes were amplified by RT-PCR from approximately 1×10^8 mononuclear cells isolated from 50 ml of peripheral blood from each patient. The phage antibody libraries were constructed by randomly combining the genes coding Fd fragments of IgG heavy chains with IgG light chain genes of either lambda or kappa DNA in equal amounts (see Supplemental Figure S1 at http://ajp.amjpathol.org.). The phagemid libraries were electroporated into *E. coli* XL1-Blue strain (Stratagene, La Jolla, CA), and the phage display of the libraries was performed as described elsewhere.[17,20] Before amplification, the resulting libraries were examined for the coexpression of heavy and light chains by enzyme digestion and for the diversity by fingerprinting of antibody genes (Fd and light chain) of 24 randomly selected single colonies.[20,21] The amplified recombinant phages were purified from culture supernatants by polyethylene glycol precipitation and resuspended in PBS, pH 7.4, containing 1% bovine serum albumin (BSA) and 10% glycerol.

Isolation of Phage Antibodies against NC16A Domain of Human COL17

Recombinant fusion peptide of the human COL17 NC16A domain (rhNC16A) with glutathione S-transferase (GST) was synthesized as reported previously.[3] Library panning was performed routinely.[20–22] Briefly, a freshly amplified phage library (approximately 1×10^{12} phages) was incubated for 2 hours at 37°C in immuno-tubes (Nunc, Roskilde, Denmark) coated with 50 μg/ml rhNC16A in 50 mmol/L $NaHCO_3$ pH 9.6. After washing of the tube with 0.05% (v/v) Tween-20 in PBS, adherent phages were eluted with 0.1 mol/L triethylamine (Sigma-Aldrich, Inc., St. Louis, MO). After neutralization with 1 mol/L Tris, pH 7.4, eluted phages were used to infect a fresh culture of XL1-Blue *E. coli*, which was amplified overnight as previously described.[20] Phages were harvested from culture supernatants and then repanned against rhNC16A for three subsequent rounds as described for the original library. Individual single ampicillin-resistant colonies resulting from infection of *E. coli* XL1-Blue with the eluted phage from the fourth panning round were isolated, and the binding to rhNC16A was confirmed by ELISA using HRP-conjugated anti-M13 mAb (Amersham Biosciences UK Ltd., Little Chalfont, Buckinghamshire, UK) as the developing reagent. The specific binders were screened by gene fingerprinting and sequencing to identify different clones. The variable region sequences of the separate selected clones were analyzed for homology to known human V, D, and J genes using the V BASE database (http://vbase.mrc-cpe.cam.ac.uk/).

Production, Purification, and Characterization of Soluble Fab

Fab Production and Purification

Plasmid DNA of the distinct selected clones was prepared, digested by *Nhel* (New England BioLabs,

Ipswich, MA) to remove the gene III fragment, self ligated, and transformed into *E. coli* XL1-Blue. Clones were grown in LB containing 100 μg/ml ampicillin, and Fab expression was induced using 1 mmol/L isopropyl β-D-thiogalactopyranoside (IPTG, Sigma) in culture grown at 30°C overnight. Cells were pelleted by centrifugation, and the supernatant containing soluble Fab was taken for analysis.

Large-scale production of Fabs was achieved by growing Fab-express clones in *E. coli* XL1-Blue in 1 L of LB (plus 100 μg/ml ampicillin). Protein production was then induced with 1 mmol/L IPTG by culturing overnight at 30°C at 240 rpm. The culture supernatant was harvested by centrifugation. Fab purification was performed using HisTrap FF crude column (GE Healthcare Bio-Sciences AB, Uppsala, Sweden) according to the manufacturer's instructions. The purified Fabs were dialyzed against PBS and concentrated by Amicon ultrafiltration (Millipore, Lexington, MA) and were then characterized by SDS-PAGE and Western blotting. For animal experiments, the concentration of endotoxin in the purified Fabs was detected with the limulus amoebocyte lysate test using the QCL-1000 kit (Cambrex Bio Science Walkersville, Inc., Walkersville, MD), and endotoxin removal was performed by using Detoxi-Gel AffinityPak column (Pierce, Rockford, IL), where necessary.

ELISA

The binding activity and specificity of Fabs was confirmed by ELISA assay. ELISA plate wells were coated with 5 μg/ml rhNC16A in 50 mmol/L $NaHCO_3$ pH 9.6. Recombinant mouse NC16A (rmNC16A), GST, and BSA were used as negative control antigens at similar concentrations. Supernatant containing Fabs or appropriately diluted purified Fabs was incubated on ELISA plates. After washing, plates were developed with HRP-conjugated mAbs to human lambda light chain (Kirkegaard & Perry Laboratories, Gaithersburg, MD) or kappa light chain (Bethyl Laboratories, Inc., Montgomery, TX) and o-phenylenediamine substrate (Wako, Osaka, Japan). Absorbance was read at 492 nm.

Western Blotting

Western blotting was performed as previously described. Briefly, recombinant proteins were electrophoresed on SDS-PAGE and electrotransferred onto nitrocellulose membrane. The blots were blocked with 5% milk in TBS/T and incubated for 1 hour with the diluted Fabs at room temperature. After washing, the blots were incubated with HRP-conjugated mAbs to human lambda light chain or kappa light chain. The bound antibodies were detected by the Phototope Western Detection Systems (Cell Signaling Technology, Inc., Danvers, MA).

Epitope Mapping

Epitope mapping studies were performed using the standard Western blotting protocol described above. The NC16A domain of human COL17 was divided into subregions as described by Giudice et al.[15,23] The expression vectors NC16A1, NC16A2, NC16A2.5, and NC16A3, which respectively correspond to amino acid segments 490 to 506, 507 to 520, 514 to 532, and 521 to 534, were gifts from Dr. George J Giudice (Medical College of Wisconsin, Milwaukee). Affinity purified products of recombinant human NC16A and its subregions were electrophoresed and electrotransferred to nitrocellulose membrane. The membranes were then probed with Fabs and allowed to react with HRP-conjugated secondary mAbs to human lambda light chain or kappa light chain.

Immunogold Electron Microscopy

Normal human skin samples were processed for postembedding immunoelectron microscopy as previously described.[24,25] Briefly, cryofixed cryosubstituted samples were embedded in Lowicryl K11M resin and polymerized at −60°C under UV light. Selected blocks were used to produce ultrathin sections that were incubated with Fabs (80 μg/ml), diluted in PBS-based buffer, and washed four times (five minutes each). Further incubations were performed using rabbit anti–c-*myc* tag antibody (Santa Cruz Biotechnology, Santa Cruz, CA) followed by four washes and further incubation with 5-nm gold-conjugated antibody for immunogold labeling (Biocell, Cardiff, UK) diluted 1 in 200 in TBS buffer. Other primary anti-COL17 antibodies included for comparison were HD4 233, 1D1, and 1A8C, each of which recognizes different domains of human COL17 (extracellular domain close to the C-terminal, mid portion, and cytoplasmic domains, respectively).[26] Sections were viewed under a Hitachi H-7100 transmission electron microscope (Hitachi, Tokyo, Japan) at 80 KV.

Immunofluorescence

Five-μm cryosections of OCT-embedded skin were cut and placed onto microscope slides and subjected to IF studies. IIF using Fabs was performed on the skin samples from human or COL17 humanized mice using a standard protocol. FITC conjugated secondary antibodies against human lambda light chain (DakoCytomation, Glostrup, Denmark), kappa light chain (Invitrogen Corp., Carlsbad, CA), or c-*myc* tag (Santa Cruz Biotechnology) were used as detection reagents.

Surface Plasmon Resonance Analysis

Affinity of the generated Fabs was determined by BIAcore assay. The on and off rate constants (k_{on} and k_{off}) for binding of the Fabs to rhNC16A were determined by a BIAcore 2000 instrument (Biacore AB, Uppsala, Sweden). For analysis of the interaction kinetics, Fabs in various concentrations (100, 80, 60, 50, and 40 nmol/L) were injected over the immobilized antigen at a flow rate of 20 μl/min using HBS-EP buffer (Biacore AB). The association and dissociation phase data were fitted simultaneously to a 1:1 Langmuir global model by using the

BIAevaluation software. The affinities (dissociation constant, K_D) were calculated from the ratio of the rate constants of association and disassociation (k_{on}/k_{off}).

Functional Analysis of Fabs in Vitro

Preparation of BP Autoantibodies

BP autoantibodies were purified from either pooled sera from 20 patients or were included as separate serum samples from three patients with active BP. Briefly, the total IgG fraction from BP sera was prepared by affinity chromatography using HiTrap Protein G HP column (Amersham Biosciences UK Limited). Then, BP autantibodies against the COL17 NC16A peptide were affinity purified from the IgG fraction using HiTrap NHS-activated HP column (Amersham Biosciences UK Ltd.) precoated with rhNC16A according to the manufacturer's instructions.[3] The NC16A affinity purified BP autoantibodies were dialyzed against PBS and concentrated by Amicon ultrafiltration (Millipore). These NC16A affinity purified BP autoantibodies were designated as BP antibodies (BPAbs), and used for *in vitro* inhibition experiments.

For the *in vivo* experiments using whole BP-IgG fractions as the pathogenic autoantibodies, serum samples were collected from another 10 BP patients and total IgG fraction was prepared using HiTrap NHS-activated HP column. This was designated as BP-IgG. Binding activity with different autoantigens was tested by ELISA and Western blotting. The BP-IgG from all ten of the serum samples bound to human COL 17, and the BP-IgG from seven of the ten serum samples also reacted with BP230. The binding of the BP-IgG with the subdomains of NC16A (NC16A-1, -2, -2.5, -3, as described by Giudice et al[15]) was further studied. All ten of the serum samples bound to NC16A-2 and NC16A-2.5. In addition, two of the ten serum samples also bound to NC16A-1 or -3. When the pooled IgG from these ten patients was first incubated with the NC16A domain of COL17 overnight at 4°C, the reaction with the NC16A domain was markedly reduced, whereas binding to the full length COL17 was unchanged by Western blotting. This indicates that the BP-IgG recognize numerous epitopes on both COL17 and BP230 antigens, and that there exist autoantibodies recognizing different epitopes both within and outside of the COL17 NC16A domain.

Inhibition ELISA

To check the competition effect of Fabs on the binding of BPAbs to rhNC16A, an inhibition ELISA was performed by incubating purified BPAbs (8 μg/ml) with 0 to 32 μg/ml Fabs on rhNC16A ELISA plates. To detect the IgG autoantibodies, the plates were developed with HRP-conjugated polyclonal antibody to human IgG (DakoCytomation) and o-phenylenediamine substrate. Absorbance was read at 492 nm. The reduced reaction of BPAbs with rhNC16A was expressed as an inhibition rate, which was calculated according to the following formula: inhibition rate % = (A492*b* − A492*f*)/A492*b* × 100, where A492*b* is the reaction with BPAbs only and A492*f* is the reaction competed with Fab at a given concentration.

Inhibition ELISA between phage antibodies (Phabs) and Fabs from the isolated clones was performed to determine whether the Fabs against different epitopes mutually cross-inhibit binding by steric hindrance. Individual Phabs were incubated with rhNC16A on ELISA plates. The reaction was challenged with Fabs from different clones at various concentrations. After washing, the remaining binding of the Phabs to rhNC16A was developed with the HRP-conjugated anti-M13 antibody and o-phenylenediamine substrate.

Inhibition IF

Inhibition IF was assessed to check the competition of Fabs to the binding of BPAbs by incubating purified BPAbs (10 μg/ml) with 0 to 40 μg/ml Fabs on human skin sections. FITC-conjugated anti-human IgG (DakoCytomation) was the detection reagent. The inhibition IF was also performed by sequential incubation with BPAbs on human skin sections, which was followed by Fabs with a 30-minute interval. The effects of Fab inhibition on the binding of autoantibodies from patients with linear IgA bullous dermatosis and anti-p200 pemphigoid were also observed.

In Vitro *Inhibition of BPAb-Induced Complement Activation*

BPAb-induced complement activation in human skin samples and the inhibitory effects of anti-COL17 NC16A Fabs were observed by IF as described by Nelson et al with minor modifications.[9] Cryosections of normal human skin were incubated with BPAbs (10 μg/ml), anti-COL17 NC16A Fabs (10 to 40 μg/ml), or BPAbs plus anti-COL17 NC16A Fabs for one hour at 37°C. Freshly prepared normal human serum was then added as a complete complement source. One hour after incubation, *in situ* deposition of human C1q and C3 at the DEJ was detected with FITC-conjugated mAbs to human C1q and human C3 (DakoCytomation), respectively.

Effects of Fabs on BP Mouse Model in Vivo

All mouse procedures were approved by the Institutional Animal Care and Use Committee of Hokkaido University, and the experimental mice were housed in a specific pathogen-free animal facility. The BP model mice were produced by injecting BP autoantibodies, either NC16A affinity purified BPAbs (50 μg/g body weight) or whole BP-IgG (1 mg/g body weight) prepared from BP patients, into the COL17 humanized neonatal mice, as previously reported.[3] At 48 hours after the injection, the mice developed human BP-like clinical and histological characteristics with serum autoantibody titers ranging from 1:80 to 1:640 in IIF and a mean BP180 antibody index value of 55.7 ± 21.1 by ELISA measurement, which is similar to the autoantibody level usually found in the sera of active BP patients. To observe the effects of the generated

anti-COL17 NC16A Fabs on the COL17 humanized mice and on the BPAb-induced disease, we divided the neonatal mice into different groups. We first injected Fabs from the three individual clones to test whether the recombinant Fabs themselves are pathogenic in COL17 humanized mice. The Fab doses were 30 to 90 μg/g body weight (30 μg/g body weight is roughly an equimolar dose compared with 50 μg/g body weight of IgG-BPAbs). To sequentially monitor the serum Fab levels after injection, 60 μg/g body weight of Fab-B4 was injected into the neonatal mice and blood samples were collected by sacrificing mice at 6, 24, 48, and 72 hours. The Fab concentration was quantified using a sandwich ELISA technique with two mAbs. To capture Fabs in the samples, rabbit anti-c-*myc* mAb (Santa Cruz Biotechnology) was coated onto ELISA plates (20 μg/ml in PBS overnight at 4°C). After blocking with 3% BSA for one hour at 37°C, individual serum samples were diluted with 1% BSA in PBS buffer (1:10) and incubated for 1 hour at 37°C. Purified Fab was used as a standard at concentrations ranging between 0.1 μg/ml and 50 μg/ml. The plate was then incubated with HRP-conjugated mouse anti-human lambda light-chain mAb to detect the reaction. The concentrations of Fabs in the samples were calculated from the standard curve for each plate.

The effects of Fabs on the BP autoantibody-induced mouse model were observed by injecting Fabs either from individual clones or from various combinations of the clones. The injection of antibodies into mice was performed as described previously, with minor modifications.[3] Briefly, each mouse received a single intraperitoneal injection of different antibodies according to group. At 48 hours after injection, the extent of skin disease was judged, including distinct Nikolsky sign. The animals were then sacrificed, and skin samples were studied by light microscopy and direct immunofluorescence microscopy using FITC conjugated antibodies against human lambda light chain (DakoCytomation), c-*myc* tag (Santa Cruz Biotechnology), human IgG (Jackson, West Grove, PA), and mouse complement C3 (Cappel, ICN Pharmaceuticals, Inc., Aurora, OH). The quantification of mast cells (MCs) and MC degranulation was performed as described by Nelson et al, and the results were expressed as a percentage of degranulated MCs (number of degranulated MCs per total number of MCs in 5 random fields × 100%).[9]

Blood was collected, and the serum sample was prepared and used for ELISA to determine the titers of circulating BPAbs or Fabs. The level of BPAbs in the serum samples of experimental mice was tested using an anti-COL17 ELISA kit according to the manufacturer's instructions (MBL, Nagoya, Japan). Absorbance was read at 450 nm. The index value was defined by the following formula: index = (A450 of tested serum − A450 of negative control)/(A450 of positive control − A450 of negative control) × 100. The concentration of the recombinant Fabs in serum samples obtained from the experimental mice was quantified using the sandwich ELISA technique described above.

Statistical Analysis and Ethical Considerations

Differences in the ELISA inhibition results among various groups were examined for statistical significance using the analysis of variance with Fisher PLSD test. For the analysis of MC degranulation among various groups of Fab treatments, we determined statistical significance using multiple tests including the Student *t* test and one way analysis of variance. *P* values less than 0.05 were considered significant.

This study was approved by the Institutional Review Board of Hokkaido University, and fully informed consent from all patients was obtained for use of human material.

Results

Isolation of Anti-COL17 NC16A Antibodies from Phage Antibody Libraries

Two individual Fab phage libraries containing 8 × 10^7 clones and 4 × 10^7 clones, respectively, were successfully constructed by combining light chain genes and heavy chain genes amplified from antibody repertoires of two BP patients (library 1 from patient 1; library 2 from

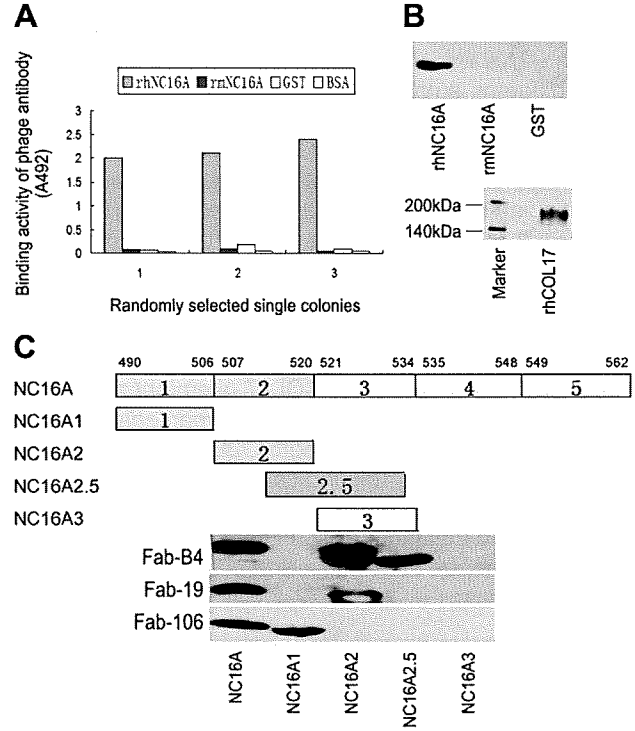

Figure 1. Isolation of specific binders against the NC16A domain of human type XVII collagen from phage antibody library. **A:** Randomly selected single colonies from the fourth panning round of the libraries show positive reaction with recombinant human NC16A (rhNC16A) but no reaction with recombinant mouse NC16A (rmNC16A), GST, or BSA in ELISA. **B:** Western blotting of soluble Fabs shows staining of only the rhNC16A domain and full-length human COL17, whereas rmNC16A and GST are negative. The representative results using Fab-B4 are shown. **C:** Epitope mapping of the generated Fabs with rhNC16A and its subdomains are shown. Fab-B4 binds to rhNC16A, NC16A2, and NC16A2.5 but does not react with NC16A1 and NC16A3, indicating that the binding epitope is located within an overlapping region within subdomain 2 and 2.5 (amino acids 514 to 520). The Fab-106 and Fab-19 epitopes are located in subdomain 1 (NC16A1, amino acids 490 to 506) and subdomain 2 (NC16A2, amino acids 507 to 520), respectively.

Table 2. Heavy and Light Chain Genes of Isolated Fabs

Fab clone	VH family	Amino acid sequences of VH			VL family	Amino acid sequences of VL		
		CDR1	CDR2	CDR3		CDR1	CDR2	CDR3
B4	VH1	NYAFSW	GIIPMSGEGHKAQKFQG	PSRSNYAGGMDV	Vλ1	SGSSSNIGRHYVY	TNYRRPS	ASWDDSL
B12	VH3	SYSMN	SISSSSSYIYYADSVKG	IDSSSWYEGWFDP	Vλ1	SGSTSNIGSNTVN	SNNQRLS	GTWDDSLN
B21	VH3	SYVLS	LLVVMLEADTTQTPEG	GNNWYGQTFDF	Vλ1	GAAPTSGQVMMYTW	GNSNRPS	QSYDSSLS
F32	VH3	SYAMH	VISYDGSNKYYADSVKG	ALRGYSYGT	Vκ1	RASQSISSYLN	AASSLQS	QQSYSLF
19	VH3	NYGMH	VISYDGSKKYYADSVKG	GFYYDWGTYYDY	Vλ1	TGSSSNIGAGYDVH	ANSNRPS	QSYDSSLT
106	VH3	DSAIH	RVRSKTNNYATDYAVSVKGR	HGESRSWYVGSGYWFDP	Vλ1	SGSSSNIGNNYVS	DNNKRPS	GTWDSSLS

Six unique antibody clones against the NC16A domain of human COL17 were identified by sequencing the heavy and light chain variable regions. Of these, clones B4, B12, B21, and F32 were isolated from library 1, whereas clones 19 and 106 were isolated from library 2. The deduced amino acids sequences of the complementary determining regions (CDRs) are shown.

patient 2). Phabs were selected by panning against rhNC16A immobilized on immune tubes. ELISA of the Phabs revealed specific positive reactions with rhNC16A in 40 of 96 and 32 of 80 colonies isolated from the two libraries, respectively (Figure 1A). By BstN I fingerprinting and sequencing of variable regions of heavy chain (VH) and light chain (VL) genes, nine unique antibody clones against rhNC16A were identified and were allowed to express the soluble Fab fragments.

Expression and Characterization of Fabs

Soluble Fab fragments of the nine antibody clones were successfully expressed by removing the gene III fragment of the phagemid vector. Four of the soluble Fabs from library 1 (Fab-B4, Fab-B12, Fab-B21, Fab-F32) and two from library 2 (Fab-19, Fab-106) were highly specific to rhNC16A in ELISA (data not shown) and Western blot analysis (Figure 1B, representative Western blot result). The other three clones, however, could not be detected as soluble fragments, probably because of their low affinity. The VH and VL genes of the six positive Fab clones are summarized in Table 2.

By epitope mapping, the binding site of the Fabs with rhNC16A and its subdomains was obtained. All four of the Fabs from library 1 showed the same reactive pattern. They bound to rhNC16A and subdomains 2 and 2.5 but failed to react with subdomains 1 and 3, indicating that their binding epitope was within the overlapping region (amino acids 514 to 520) of subdomains 2 and 2.5. The two Fabs from library 2 bound to different subdomains: Fab-106 reacted only with subdomain 1 (amino acids 490 to 506) and Fab-19 reacted only with subdomain 2 (amino acids 507 to 520). This indicates that they bound to different epitopes on COL17 NC16A. The representative blot results are shown in Figure 1C. These data demonstrate the successful isolation of anti-COL17 NC16A Fabs from patients with BP.

We chose Fabs (Fab-B4, Fab-19, and Fab-106) that had been raised against different epitopes of COL17 NC16A for further experiments. All of the light chains of these three clones are from human lambda light chain family. Large-scale production was performed, and a yield of approximately 1 to 3 mg of Fab product was obtained from each 1 L culture after column purification. Figure 2A shows the SDS-PAGE identification of the purified Fab in reduced and nonreduced form.

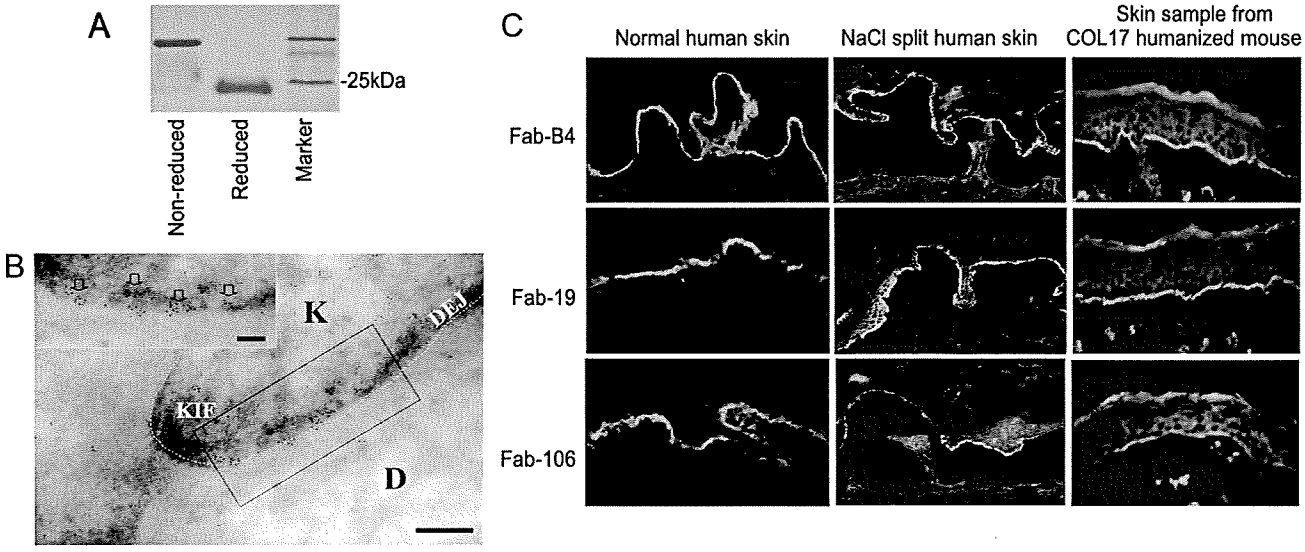

Figure 2. Production and characterization of Fabs. **A:** A purified soluble Fab in both reduced and nonreduced states is shown by Coomassie blue staining after SDS-PAGE. **B:** Immunogold labeling of normal human skin by Fabs shows 5-nm immunogold deposits restricted to immediately beneath hemidesmosomes, close to the keratinocyte plasma membrane (**arrows**, bar = 100 nm). The representative results using Fab-B4 are shown. (**K:** keratinocyte; **D:** dermis; KIF: keratin intermediate filaments; DEJ: dermal-epidermal junction). **C:** Immunofluorescence studies on normal human skin and skin sections from COL17 humanized mice show positive staining of the selected Fabs at the DEJ, and positive staining is also noted on the roof of NaCl split skin samples.

Table 3. Affinity of Anti-COL17 NC16A Fabs Measured by BIAcore System

Fab	k_{on} (1/Ms)	k_{off} (1/s)	K_D (M)
Fab-B4	2.83×10^5	1.10×10^{-3}	3.89×10^{-9}
Fab-19	1.14×10^5	6.26×10^{-3}	5.48×10^{-8}
Fab-106	5.52×10^5	8.08×10^{-2}	1.46×10^{-7}

Kinetic parameters k_{on} and k_{off} were measured by BIAcore system, and K_D was calculated as k_{on}/k_{off}. From the three Fabs, Fab-B4 has the highest affinity.

Immunogold electron microscopy showed that 5-nm immunogold particles were restricted to immediately beneath hemidesmosomes, below the keratinocyte plasma membrane (Figure 2B). Mean measurements of immunogold deposits demonstrated that their epitopes were about 1 to 2 nm (mean 1.77 nm ± SD, $n > 200$) beneath the plasma membrane and located between the epitopes of 1A8C, a cytoplasmic plaque associated COL17 antibody) and 233 (an extracellular COL17 antibody), as described by Nonaka et al.[26] No difference in distribution of the immunogold deposits was found between the three Fabs.

In the IIF experiments, as we expected, all three Fabs showed linear deposition at the DEJ and positive staining was noted along the roof of the NaCl split skin samples, consistent with COL17 staining (Figure 2C).

Kinetic analysis using the BIAcore system demonstrated affinity levels of Fab-B4, Fab-19, and Fab-106, as summarized in Table 3. Among these Fabs, Fab-B4 showed the highest affinity value and Fab-106 showed the lowest.

Functional Analysis of Fabs in Vitro

To determine whether the Fabs generated against COL17 NC16A were able to function in competitive binding to inhibit the emergence of an autoantibody-mediated BP phenotype, we initially performed a series of *in vitro* experiments to evaluate their ability to block BP autoantibody binding to COL17. Figure 3A shows that the rhNC16A binding activities of BPAbs, which were affinity purified using recombinant COL17 NC16A peptide from the pooled sera from 20 BP patients, were reduced markedly and significantly by Fab-B4 and Fab-19, but only marginally by Fab-106, in a dose-dependent manner (0 to 32 μg/ml). Fab-B4 and 19 suppressed the binding of BPAbs most efficiently at a concentration of 32 μg/ml, with the highest inhibition rates of 52.4% and 50.8%, respectively. Combinations of two or three Fabs failed to increase this inhibition efficacy. When tested with BPAbs isolated from individual BP patients, Fabs showed similar competitive effects (Figure 3B).

IIF studies show competitive blocking of Fabs with BPAbs on skin sections. Figure 4 shows positive IgG

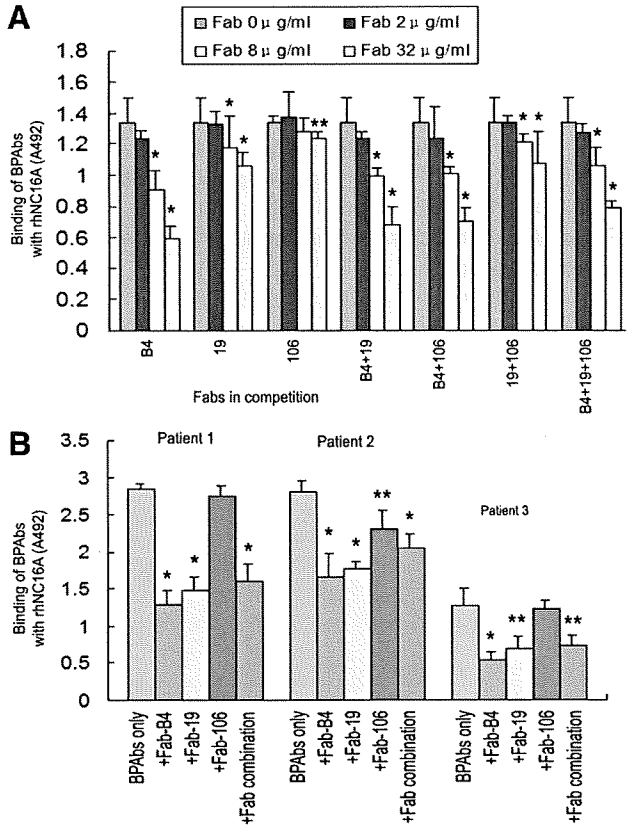

Figure 3. Inhibition ELISA assay. **A:** The effects of competition with Fab-B4, Fab-19, and various combinations inhibit the binding of autoantibodies (BPAbs, 8 μg/ml) from pooled sera of patients with bullous pemphigoid (BP) to rhNC16A in a dose-dependent manner (0 to 32 μg/ml), whereas Fab-106 inhibits BPAb binding only moderately. $^*P < 0.01$, $^{**}P < 0.05$, versus the original binding of BPAbs. **B:** Fabs (32 μg/ml) inhibit the binding of BPAbs from three BP patients. $^*P < 0.01$, $^{**}P < 0.05$, versus the original binding of BPAbs.

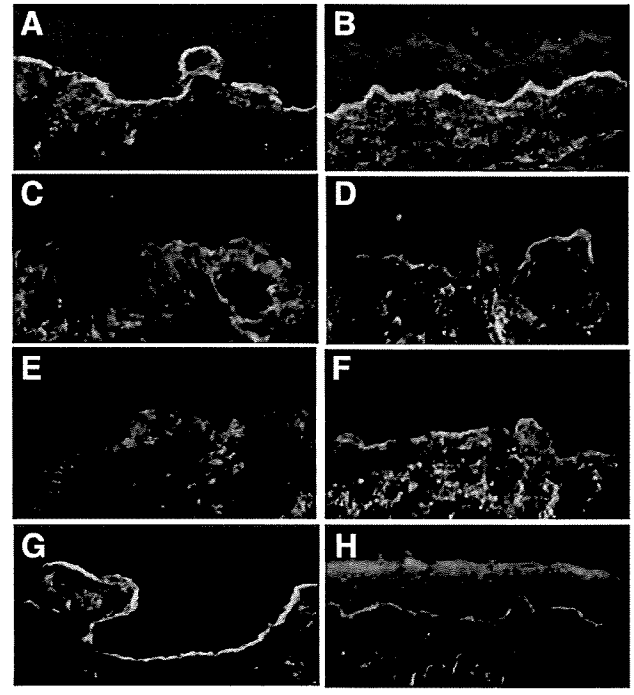

Figure 4. Inhibition immunofluorescence. **A** and **B:** Positive IgG staining of the NC16A affinity purified BPAbs (10 μg/ml) at the DEJ in human skin. **C** and **E:** IgG BPAbs staining is blocked by coincubation with either Fab-B4 or Fab-19 at a concentration of 20 μg/ml. **G:** Fab-106 (20 μg/ml) fails to significantly inhibit the binding of BPAbs. When BPAbs are allowed to bind to skin sections first and Fabs are added 30 minutes later, the IF staining of BPAb binding is also markedly reduced by Fab-B4 (**D**) or Fab-19 (**F**) but not by Fab-106 (**H**).

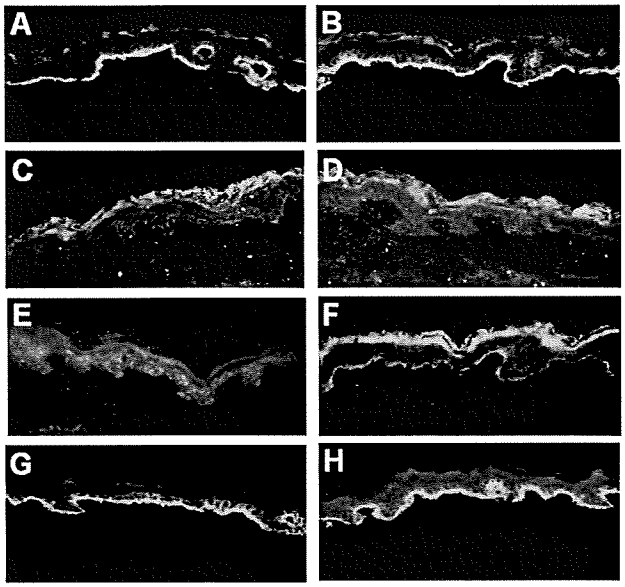

Figure 5. BPAb-induced complement activation and the inhibitory effects of Fabs. NC16A affinity purified BPAbs (10 μg/ml) induced activation of human C1q and C3 is shown at the DEJ in cryosections of human skin (**A** and **B**). When Fabs are coadministered with BPAbs at the same concentration, Fab-B4 completely blocks C1q and C3 activation (**C** and **D**), whereas Fab-19 effectively blocks the activation of C1q (**E**) and markedly reduces the activation of C3 (**F**). Fab-106 shows no inhibition of either C1q or C3 activation (**G** and **H**).

BPAbs staining (10 μg/ml) at the DEJ in human skin (Figure 4A), which was blocked by coincubation with either Fab-B4 or Fab-19 at a concentration of 20 μg/ml (Figure 4, C and E). Fab-106 failed to significantly inhibit the binding of BPAbs (Figure 4G). When BPAbs were allowed to bind to skin sections first and Fabs were added 30 minutes later, the IF staining of BPAb binding was also markedly reduced although not completely inhibited (Figure 4, B, D, F, and H). Competitive IF using Fabs and individual patient BPAbs showed that Fab-B4 and Fab-19 were able to block the binding of autoantibodies from three individual BP patients, whereas none of the Fabs inhibited the binding of IgA autoantibodies from patients with linear IgA bullous dermatosis or IgG autoantibodies from patients with anti-p200 pemphigoid (data not shown).

In vitro inhibition of complement activation by recombinant Fabs was studied by immunofluorescence. *In situ* deposition of BPAb-activated C1q (Figure 5A) and C3 (Figure 5B) was found at the DEJ in human skin. Complement deposition was reduced or completely blocked by Fab-B4 (Figure 5, C and D) or Fab-19 (Figure 5, E and F), whereas it was unchanged by Fab-106 treatment (Figure 5, G and H). Fabs against COL17 NC16A did not activate complement at concentrations up to 100 μg/ml.

We also tested the effect of competition between recombinant anti-COL17 NC16A Fabs. Using an inhibition ELISA, Fabs from the three clones inhibited the binding of Phabs from their own clone as we might have expected. Interestingly, Fab-B4 and Fab-19 cross-inhibited each other while Fab-106 failed to inhibit the other two (Figure 6, A–C). These data indicate that Fab-B4 and Fab-19 specifically recognize distinct but close or overlapping

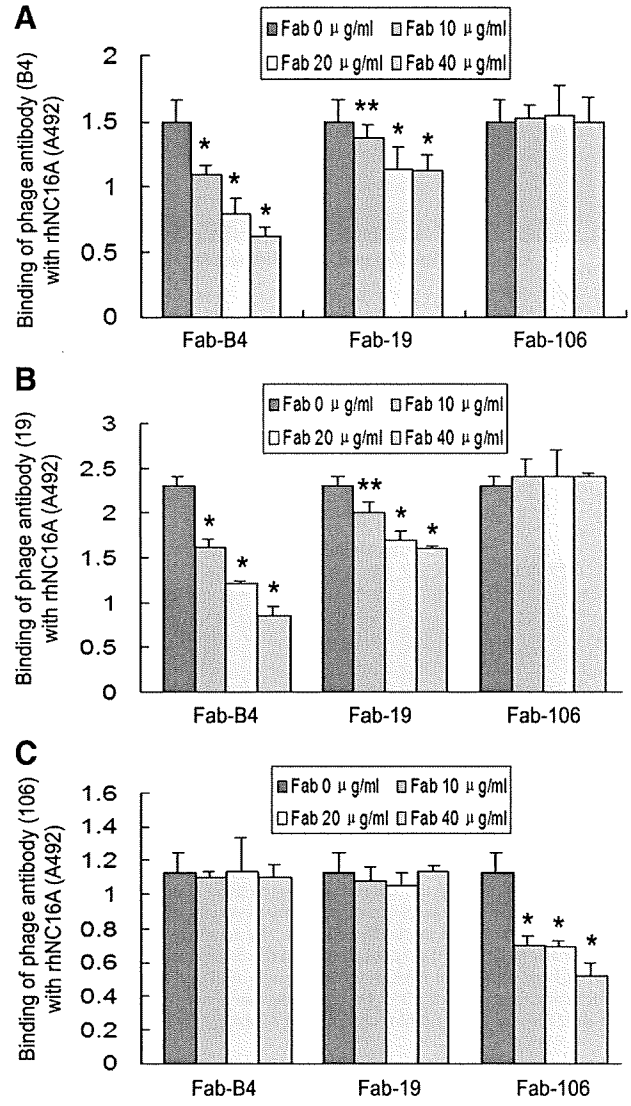

Figure 6. Inhibition ELISA for the three recombinant antibody clones using Fabs and phage antibodies (Phabs). Fab-B4 and Fab-19 inhibited the binding of both Phab-B4 and Phab-19 (**A** and **B**), whereas Fab-106 inhibited Phab-106 only (**C**). This indicates that the antibody clones B4 and 19 are mutually cross-inhibiting. $^{*}P < 0.01$, $^{**}P < 0.05$, versus the original binding of respective Phabs.

epitopes and are able to block the binding of BP antibodies in nearby epitopes, most likely by direct steric hindrance.

In Vivo *Blockade of Autoantibody-Induced BP Disease*

We first proved that recombinant Fabs were not pathogenic to COL17 humanized mice after injection with 30 to 90 μg/g body weight of Fab-B4, -19, or -106 into neonatal mice. Neither clinical signs, including erythema and Nikolsky sign, nor any histopathological manifestations of BP were found in the treated mice. Direct immunofluorescence studies demonstrated clear deposition of the recombinant Fab fragments at the DEJ. Subsequent deposition of mouse C3 was not detected (Figure 7A).

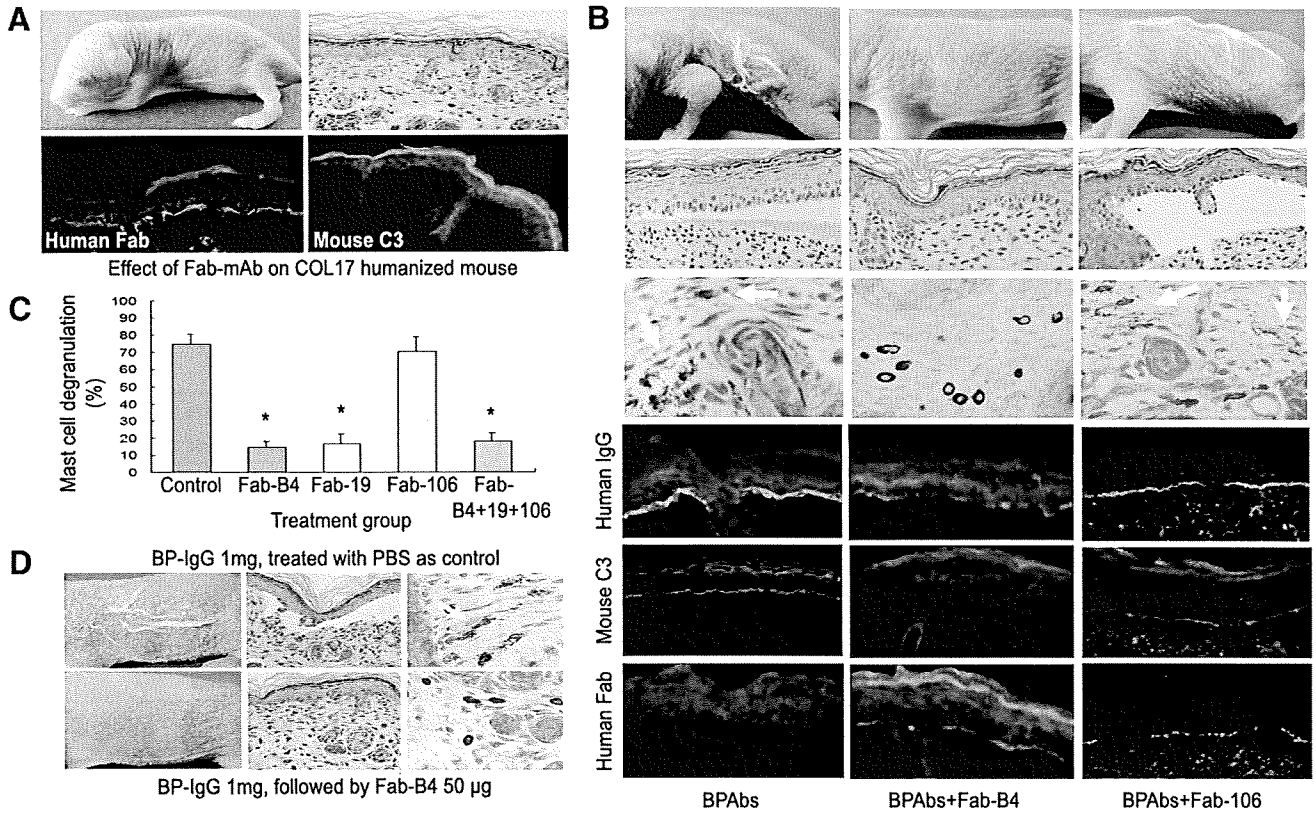

Figure 7. Therapeutic effects of Fabs on BP model mice. **A:** Results of the injection of Fabs into neonatal COL17 humanized mice show that this treatment alone does not cause BP disease or other detectable adverse effects. Histological examination (**right, upper panel**) supports this result. Indirect immunofluorescence show DEJ staining for the recombinant Fabs (**left** of **lower panel**) but no staining for mouse C3 (**right, lower panel**). **B:** Mice injected with NC16A affinity purified BPAbs develop the clinical and histological skin detachment associated with MC degranulation (**white arrows**) and the deposition of human IgG and mouse C3 at the DEJ. In contrast, mice injected with BPAbs and Fab-B4 fail to show these clinical and histological characteristics, and the intensity of IgG deposition at the DEJ is markedly reduced. The staining of mouse C3 is absent, whereas recombinant Fab fragment staining is weak but detectable. Fab-106 fails to show any beneficial therapeutic effect in the animal model. **C:** Percentage of dermal MC degranulation is assessed in BP model mice and in those treated with 30 μg/g body weight of Fabs. It is significantly reduced in the mice treated with Fab-B4, Fab-19, and the Fab combination. $^*P < 0.01$ versus control group (BP model mice treated with PBS). **D:** BP model mice were produced by injection of BP-IgG (total IgG fraction prepared from BP patients) and were treated with Fab-B4 24 hours later. BP-like clinical and histological characteristics fail to develop in most (four of five) of Fab-B4 treated mice (**lower panel**).

For further *in vivo* experiments, we again used the humanized BP mouse model and induced disease by injecting BP autoantibodies, either BPAbs (50 μg/g body weight) or whole BP-IgG (1 mg/g body weight), into neonatal COL17 humanized mice. We sequentially analyzed the serum concentration of BP autoantibodies in the injected mice. Their autoantibody titers ranged from 1:80 to 1:640 in IIF, and the mean BP180 antibody index value reached the highest level of 72.8 ± 21.7 at 6 hours and then gradually decreased to 68.5 ± 9.1 at 12 hours, 64.1 ± 14.9 at 24 hours, 55.7 ± 21.1 at 48 hours, 33.4 ± 4.8 at 72 hours, and 33.7 ± 2.6 at 96 hours after injection. After i.p. injection of BPAbs or whole BP-IgG, the mice were i.p. treated either immediately or 24 hours later with Fabs from each of the three individual clones. The results were evaluated 48 hours later (Table 4). As shown in Figure 7B, the BP model mice untreated with Fabs demonstrated a BP-like clinical phenotype with extensive erythema and Nikolsky sign together with histological characteristics, including dermal-epidermal separation and the infiltration of inflammatory cells. These clinical and histological signs failed to develop in any of the Fab-B4 groups, including the immediately treated and the 24 hour–treated mice. Treatment with Fab-19 demonstrated a similar effect. Fab-106, however, failed to show any therapeutic efficacy. Histologically, no subepidermal blister formation was found in skin samples from mice treated with Fab-B4 or -19 at a dosage of 30 μg/g body weight or higher, whereas distinctive BP-like blister formation was observed in skin sections from the majority of the Fab-106 treated mice (4/5 mice with the 30 μg/g body weight treatment and 4/4 mice with the 60 μg/g body weight treatment) or control mice. Fab combination therapy at the same total dose showed a similar result as treatment with Fab-B4 or -19 alone. Direct immunofluorescence studies revealed that deposition of human IgG and mouse C3 at the DEJ was significantly reduced in the Fab-B4 or -19 treated groups compared with that of controls. Extensive MC degranulation took place in the dermis of the BP model mice. In contrast, the percentage of degranulated MCs was significantly decreased in the Fab-B4– and -19–treated mice (Figure 7C). Figure 7D shows the BP disease phenotype induced by injection of whole BP-IgG (upper panel) and the therapeutic results of Fab (lower panel). Fab-B4 treatment inhibited the BP-IgG–induced phenotypic changes in all immediately treated mice, as well as the majority of the mice (4/5) treated 24 hours after the initial BP-IgG injection. To-

Table 4. Effects of Anti-COL17 NC16A Fabs on BP Autoantibody-Induced Mouse Model

Abs used for reproducing mouse model	Treatment	Total dose of Fab (μg/g body weight)	Skin detachment
COL17 NC16A- affinity purified BP autoantibodies (BPAbs)	Fab-B4	15	2/8
		30	0/10
		30 (24 hours later)	0/4
		60	0/9
	Fab-19	15	2/6
		30	0/6
		60	0/6
	Fab-106	15	5/5
		30	4/5
		60	4/4
	Fab combination (Fab-B4 + 19 + 106)	15	2/5
		30	0/6
		60	0/5
	Control	PBS	14/14
Whole IgG fractions (BP-IgG)	Fab-B4	30	0/4
		30 (24 hours later)	1/5
	Control	PBS	4/4

Neonatal COL17 humanized BP model mice were injected with either COL17 NC16A-affinity purified BP autoantibodies (BPAbs: 50 μg/g body weight) or whole IgG fractions (BP-IgG: 1 mg/g body weight) from patients with bullous pemphigoid. The mice were then treated immediately or 24 hours later (underlined) with Fabs by intraperitoneal injection. For Fab combination therapy, the total dose comprised one third of each Fab clone.

gether with the *in vitro* inhibition IF data, these results demonstrate that Fabs can at least partially displace the bound BP autoantibodies within the DEJ and block BP disease after initial binding not only by NC16A-purified BPAbs but also by combined whole IgG sera fractions from BP patients. When the mice were sacrificed at 48 hours, serum samples were collected to detect BP antibody index values and the recombinant Fab level. The BP180 antibody index value in the control mice sera was 170.3 ± 26.2, and no significant increase or decrease was found in any of the treatment groups ($P > 0.05$). The concentrations of Fabs ranged from 1.34 ± 0.11 μg/ml to 10.22 ± 0.35 μg/ml, increasing with increasing injected dose; however, there was no significant difference between the mice injected with Fabs only and the BP model mice treated with Fabs at the same given doses ($P > 0.05$). No adverse reactions to the Fab treatments were observed.

Discussion

In the present study, we successfully generated Fabs against the human COL17 NC16A domain from phage display antibody repertoires derived from two BP patients. These Fabs specifically recognize different epitopes located in NC16A subdomains and competitively inhibit the binding of human BP autoantibodies to COL17. Our novel anti-COL17 NC16A Fabs were observed to inhibit the changes in the BP mouse model that would otherwise have been induced by the injection of human BP autoantibodies into recently engineered COL17-humanized mice.

BP is the most common autoimmune blistering skin disease. The mortality rate of BP in various reports ranges from 20% to 40%, and death is more commonly related to other underlying illness, debilitation associated with severe BP condition, or adverse effects of treatment.[27] Autoantibodies against two hemidesmosomal antigens, BPAG1 (BP230) and BPAG2 (COL17 or BP180), have been identified in BP. COL17 autoantibodies are generally thought to play a critical role in the initial pathogenesis of the disease. COL17, a type II transmembrane protein, is the main pathogenic target for BP autoantibodies and the NC16A domain was subsequently confirmed as the main binding epitope.[15,28–30] COL17 autoantibodies have been widely studied and have been shown to induce activation of complement via a classical pathway that is essential for disease development. This allowed us to devise a new approach toward treating BP and a therapeutic strategy for such treatment. Using molecular and recombinant protein techniques, we identified three Fabs, Fab-B4, Fab-19, and Fab-106, which recognize multiple epitopes within the COL17 NC16A domain with different affinity levels. Of these, Fab-B4 and Fab-19 recognized distinct epitopes located within subdomain 2 of NC16A, whereas Fab-106 recognized an epitope in subdomain 1. Interestingly, Fab-B4 and Fab-19 inhibited each other in competition ELISA assays using reciprocal Phabs and soluble Fabs, indicating that they bind specifically to their corresponding epitopes and may involve mutual steric hindrance. Fab-106 showed no inhibitory effects on the other two Fabs, confirming its unique binding domain.

Fab-B4 and Fab-19, but not Fab-106, showed therapeutic potential for BP in both *in vitro* and *in vivo* studies. Both fragments competitively inhibit the binding of BP autoantibodies to the main COL17 NC16A epitope, and both of them block BPAb-mediated activation of complement C1q and C3. In our BP animal model using the COL17 humanized mouse, marked inhibition of the BP phenotype, including deposition of BPAbs and complement, degranulation of MCs, and subcutaneous blister formation, was observed in Fab-B4– or Fab-19–treated mice. It appears from these data that complete blocking of BP autoantibodies by Fabs is not required to significantly inhibit disease severity. We know this because

successful treatment of the BP model mouse was achieved even with partial blocking of BP autoantibody binding. This is consistent with the clinical observation that BP symptoms can markedly improve as the autoantibody levels gradually decrease, although autoantibodies are still detectable.[31,32] This suggests that there may be a threshold for BP autoantibodies to initiate and maintain complement activation and complement-mediated tissue injury. Partially reducing autoantibody deposition using blocking Fabs might be beneficial in alleviating BP. Furthermore, our Fab was demonstrated to be able to displace the bound BP autoantibodies both *in vitro* and *in vivo*. These results strongly support our approach of using inhibitory anti-COL17 NC16A Fabs for BP therapy. When comparing the *in vitro* and *in vivo* activities of all these Fabs together, the Fab-B4 clone appears to be most efficient. We assessed the effects of combining these three Fabs, but we failed to improve on the results. The inhibitory effect of Fab clones in combination was not as good as that of the Fab-B4 clone alone, even at equivalent dosages. The administration of Fabs themselves or in combination failed to elicit any adverse pathological manifestation in the COL17 humanized mice.

It has been shown that the majority of anti-COL17 autoantibody pathogenic epitopes are mainly distributed in subdomains 1 to 3 of NC16A.[33] Fairley et al[23] further defined subdomain 2 as the major epitope recognized by both IgG and IgE autoantibodies from BP patients. We tested the reactivity of BP autoantibodies and found that the binding amount and affinity against subdomain 2 was higher than the binding amount and affinity for subdomains 1 and 3 (data not shown). Taken together with the fact that anti-subdomain 2 Fabs show excellent therapeutic effects in BP model mice, even after the disease was induced not only by the COL17 NC16A affinity purified BPAbs, but also by whole BP-IgG fractions, we speculate that the BP autoantibodies that recognize the non-NC16A epitopes may be less pathogenic than those that recognize the NC16A epitopes. The BP autoantibodies that recognize NC16A, especially the subdomain 2 region, are the main pathogenic autoantibodies in BP. Previously reported *in vitro* studies using cryosections[34] and *in vivo* animal models[10] both suggested that anti NC16A autoantibodies are major pathogenic antibodies in BP, which further supports our speculation.

Thus far, the complement system has been an attractive therapeutic target for a wide range of autoimmune and inflammatory diseases.[2,13] There are different strategies of inhibiting complement activation. In a previous study, we tried using a recombinant peptide containing BP pathogenic epitopes as a decoy to block both the binding of BP autoantibodies and the activation of complement.[3] Although it proved effective, a potential pitfall exists. The peptide may act as an antigen and trigger a more severe immune response, and hence, result in further production of pathogenic autoantibodies. Fab therapy eliminates such concerns. Furthermore, it is highly disease-specific and does not involve systemic immune suppression; therefore, it may be used either as an individual therapy or in combination with other currently available treatments to promote efficacy and reduce adverse reactions. Our success in generating these Fabs with therapeutic potential makes it possible to create not only a more specific therapy for BP but also further potential strategies for the treatment of many other antibody-initiated complement-mediated autoimmune disorders.

Acknowledgments

We thank Ms. Noriko Ikeda, Ms. Maki Goto, Ms. Megumi Sato, and Ms. Akari Nagasaki for their technical assistance.

References

1. Jacobson DL, Gange SJ, Rose NR, Graham NM: Epidemiology and estimated population burden of selected autoimmune diseases in the United States. Clin Immunol Immunopathol 1997, 84:223–243
2. Holers VM: The complement system as a therapeutic target in autoimmunity. Clin Immunol 2003,107:140–151
3. Nishie W, Sawamura D, Goto M, Ito K, Shibaki A, McMillan JR, Sakai K, Nakamura H, Olasz E, Yancey KB, Akiyama M, Shimizu H: Humanization of autoantigen. Nat Med 2007, 13:378–383
4. Liu Z, Giudice GJ, Swartz SJ, Fairley JA, Till GO, Troy JL, Diaz LA: The role of complement in experimental bullous pemphigoid. J Clin Invest 1995, 95:1539–1544
5. Mewar D, Wilson AG: Autoantibodies in rheumatoid arthritis: a review. Biomed Pharmacother 2006, 60:648–655
6. D'Cruz DP, Khamashta MA, Hughes GRV: Systemic lupus erythematosus. Lancet 2007, 369:587–596
7. Girardi G, Berman J, Redecha P, Spruce L, Thurman JM, Kraus D, Hollmann TJ, Casali P, Caroll MC, Wetsel RA, Lambris JD, Holers VM, Salmon JE: Complement C5a receptors and neutrophils mediate fetal injury in the antiphospholipid syndrome. J Clin Invest 2003, 112:1644–1654
8. Zhao M, Trimbeger ME, Li N, Diaz LA, Shapiro SD, Liu Z: Role of FcRs in animal model of autoimmune bullous pemphigoid. J Immunol 2006, 177:3398–3405
9. Nelson KC, Zhao M, Schroeder PR, Li N, Wetse RA, Diaz LA, Liu Z: Role of different pathways of the complement cascade in experimental bullous pemphigoid. J Clin Invest 2006, 116:2892–2900
10. Liu Z, Diaz LA, Troy JL, Taylor AF, Emery DJ, Fairley JA, Giudice GJ: A passive transfer model of the organ-specific autoimmune disease, bullous pemphigoid, using antibodies generated against the hemidesmosomal antigen BP180. J Clin Invest 1993, 92:2480–2488
11. Liu Z: Bullous Pemphigoid: Using animal models to study the immunopathology. J Investig Dermatol Symp Proc 2004, 9:41–46
12. Yancey KB: The pathophysiology of autoimmune blistering diseases. J Clin Invest 2005, 115:825–828
13. Girardi G, Redecha P, Salmon JE: Heparin prevents antiphospholipid antibody-induced fetal loss by inhibiting complement activation. Nat Med 2004, 10:1222–1226
14. Atkinson JP: Complement system on the attack in autoimmunity. J Clin Invest 2003, 112:1639–1641
15. Giudice GJ, Emery DJ, Zelickson BD, Anhalt GJ, Liu Z, Diaz LA: Bullous pemphigoid and herpes gestationis autoantibodies recognize a common non-collagenous site on the BP180 ectodomain. J Immunol 1993, 151:5742–5750
16. Wang Z, Wang Y, Li Z, Li J, Dong Z: Humanization of a mouse monoclonal antibody neutralizing TNF-α by guided selection. J Immunol Methods 2000, 241:171–184
17. Barbas III CF, Kang AS, Lerner RA, Benkovic SJ: Assembly of combinatorial antibody libraries on phage surfaces: The gene III site. Proc Natl Acad Sci USA 1991, 88:7978–7982
18. Little M, Breitling F, Dubel S, Fuchs P, Braunagel M: Human antibody libraries in Escherichia coli. J Biotechnol 1995, 41:187–195
19. Clackson T, Hoogenboom HR, Griffiths AD, Winter G: Making antibody fragments using phage display libraries. Nature 1991, 352: 624–628
20. Wang G, Liu YF, Li CY, Lu N, Gao TW, Hua B, Wang Y: Cloning and

characterization of antikeratin human antibodies using a semisynthetic phage antibody library. Arch Dermatol Res 2004, 296:270–277
21. Marks JD, Hoogenboom HR, Bonnert TP, McCafferty J, Griffiths AD, Winter G: Bypassing immunization of human antibodies from V-gene libraries displayed on phage. J Mol Biol 1991, 222:581–597
22. Hoogenboom HR: Selecting and screening recombinant antibody libraries. Nat Biotechnol 2005, 23:1105–1116
23. Fairley JA, Fu CL, Giudice GJ: Mapping the binding sites of anti-BP180 immunoglobulin E autoantibodies in bullous pemphigoid. J Invest Dermatol 2005, 125:467–472
24. Shimizu H, Masunaga T, Ishiko A, Hashimoto T, Garrod DR, Shida H, Nishikawa T: Demonstration of desmosomal antigens by electron microscopy using cryofixed and cryosubstituted skin with silver-enhanced gold probe. J Histochem Cytochem 1994, 42:687–692
25. McMillan JR, Akiyama M, Nakamura H, Shimizu H: Colocalization of multiple laminin isoforms predominantly beneath hemidesmosomes in the upper lamina densa of the epidermal basement membrane. J Histochem Cytochem 2006, 54:109–111
26. Nonaka S, Ishiko A, Masunaga T, Akiyama M, Owaribe K, Shimizu H, Nishikawa T: The extracellular domain of BPAG2 has a loop structure in the carboxy terminal flexible tail in vivo. J Invest Dermatol 2000, 115:889–892
27. Khumalo N, Kirtschig G, Middleton P, Hollis S, Wojnarowska F, Murrell D: Interventions for bullous pemphigoid. Cochrane Database Syst Rev 2005 (3):CD002292
28. Schumann H, Baetge J, Tasanen K, Wojnarowska F, Schäcke H, Zillikens D, Bruckner-Tuderman L: The shed ectodomain of collagen XVII/BP180 is targeted by autoantibodies in different blistering skin diseases. Am J Pathol 2000, 156:685–695
29. Ishiko A, Shimizu H, Kikuchi A, Ebihara T, Hashimoto T, Nishikawa T: Human autoantibodies against the 230-kD bullous pemphigoid antigen (BPAG1) bind only to the intracellular domain of the hemidesmosome, whereas those against the 180-kD bullous pemphigoid antigen (BPAG2) bind along the plasma membrane of the hemidesmosome in normal human and swine skin. J Clin Invest 1993, 91:1608–1615
30. Stanley JR: Autoantibodies against adhesion molecules and structures in blistering skin diseases. J Exp Med 1995, 181:1–4
31. Kobayashi M, Amagai M, Kuroda-Kinoshita K, Hashimoto T, Shirakata Y, Hashimoto K, Nishikawa T: BP180 ELISA using bacterial recombinant NC16a protein as a diagnostic and monitoring tool for bullous pemphigoid. J Dermatol Sci 2002, 30:224–232
32. Tsuji-Abe Y, Akiyama M, Yamanaka Y, Kikuchi T, Sato-Matsumura KC, Shimizu H: Correlation of clinical severity and ELISA indices for the NC16A domain of BP180 measured using BP180 ELISA kit in bullous pemphigoid. J Dermatol Sci 2005, 37:145–149
33. Zillikens D, Rose PA, Balding SD, Liu Z, Olague-Marchan M, Diaz LA, Giudice GJ: Tight clustering of extracellular BP180 epitopes recognized by bullous pemphigoid autoantibodies. J Invest Dermatol 1997, 109:573–579
34. Sitaru C, Schmidt E, Petermann S, Munteanu LS, Brocker EB, Zillikens D: Autoantibodies to bullous pemphigoid antigen 180 induce dermal-epidermal separation in cryosections of human skin. J Invest Dermatol 2002, 118:664–671

A Novel Active Mouse Model for Bullous Pemphigoid Targeting Humanized Pathogenic Antigen

Hideyuki Ujiie, Akihiko Shibaki, Wataru Nishie, Daisuke Sawamura, Gang Wang, Yasuki Tateishi, Qiang Li, Reine Moriuchi, Hongjiang Qiao, Hideki Nakamura, Masashi Akiyama, and Hiroshi Shimizu

Bullous pemphigoid (BP), the most common autoimmune blistering disease, is caused by autoantibodies against type XVII collagen (COL17). To establish an active stable BP animal model that demonstrates the persistent inflammatory skin lesions initiated by the anti-human COL17 Abs, we used COL17-humanized (*COL17*$^{m-/-,h+}$) mice that we recently produced. First, we generated immunodeficient *Rag-2*$^{-/-}$/COL17–humanized mice by crossing *Rag-2*$^{-/-}$ mice with COL17-humanized mice. Then, splenocytes from wild-type mice that had been immunized by grafting of human COL17-transgenic mouse skin were transferred into *Rag-2*$^{-/-}$/COL17–humanized mice. The recipient mice continuously produced anti-human COL17 IgG Abs in vivo and developed blisters and erosions corresponding to clinical, histological, and immunopathological features of BP, although eosinophil infiltration, one of the characteristic histological findings observed in BP patients, was not detected in the recipients. Although the depletion of CD8$^+$ T cells from the immunized splenocytes was found to produce no effects in the recipients, the depletion of CD4$^+$ T cells as well as CD45R$^+$ B cells was found to inhibit the production of anti-human COL17 IgG Abs in the recipients, resulting in no apparent clinical phenotype. Furthermore, we demonstrated that cyclosporin A significantly suppressed the production of anti-human COL17 IgG Abs and prevented the development of the BP phenotype in the treated recipients. Although this model in an immunodeficient mouse does not exactly reproduce the induction mechanism of BP in human patients, this unique experimental system targeting humanized pathogenic Ag allows us to investigate ongoing autoimmune responses to human molecules in experimental animal models. ***The Journal of Immunology*, 2010, 184: 2166–2174.**

To investigate the pathogenic mechanisms of autoimmune diseases, the development of animal models is essential (1, 2). However, interspecies molecular differences in autoantigens make it difficult to develop autoimmune animal disease models in some cases. We recently overcame this issue by using the unique technique of humanization of autoantigens to generate an animal model for bullous pemphigoid (BP) (1).

BP is the most common autoimmune blistering disorder that is induced by autoantibodies against type XVII collagen (COL17, also called BP180 or BPAG2), a hemidesmosomal type II transmembrane protein that spans the lamina lucida and projects into the lamina densa of the epidermal basement membrane zone (3–7). The noncollagenous 16A domain located at the membrane-proximal region of COL17 is known as the major pathogenic epitope for BP (8, 9). Our group recently generated COL17-humanized mice (*COL17*$^{m-/-,h+}$) that lack mouse COL17 but express human COL17 (hCOL17) (1). Autoantibodies from BP patients fail to recognize mouse COL17 due to differences in the amino acid sequence between human and mouse. In contrast, BP autoantibodies react to hCOL17 molecules expressed in COL17-humanized mice and induce BP-like skin lesions in the neonates. Thus, this passive-transfer BP mouse model directly demonstrated the pathogenicity of human BP autoantibodies (1). Our system makes it possible to investigate immune reactions mediated by Abs specific to human molecules even in animal models.

However, passive-transfer animal models demonstrate only transient disease activity. In this study, we have developed an active, stable BP model to further advance our knowledge of the BP pathogenic mechanisms for the dynamic process of developing chronic inflammatory skin lesions observed in BP patients. To develop such a model, we adoptively transferred the splenocytes immunized with hCOL17 into immunodeficient COL17-humanized recipients (10). This active, stable autoimmune disease model targeting humanized pathogenic Ag enables us to investigate ongoing autoimmune responses to human molecules in experimental animals.

Materials and Methods

Mice

C57BL/6J mice were purchased from Japan Clea (Hamamatsu, Japan). C57BL/6-background *Rag-2*$^{-/-}$ mice were received as a gift from the Central Institute for Experimental Animals (Kawasaki, Japan). We crossed *COL17*$^{m-/-,h+}$ (COL17-humanized) mice that we had recently generated (1) with *Rag-2*$^{-/-}$ mice. Mice that carried the heterozygous null mutations of both the *Rag-2* and mouse *Col17* genes and the transgene of human *COL17* (*Rag-2*$^{+/-}$/*COL17*$^{m+/-,h+}$) were bred to produce *Rag-2*$^{-/-}$/*COL17*$^{m-/-,h+}$ (*Rag-2*$^{-/-}$/COL17–humanized) mice. All of the animal procedures were conducted according to guidelines provided by the Hokkaido University Institutional Animal Care and Use Committee under an approved protocol.

Department of Dermatology, Hokkaido University Graduate School of Medicine, Sapporo, Japan

Received for publication September 21, 2009. Accepted for publication December 9, 2009.

This work was supported in part by Grants-in-Aid for Scientific Research (A) (No. 21249063 to H.S.) and (C) (No. 20591312 to A.S.) from the Ministry of Education, Culture, Sports, Science and Technology of Japan and by the Program for Promotion of Fundamental Studies in Health Sciences of the National Institute of Biomedical Innovation (No. 06-42 to H.S.).

Address correspondence and reprint requests to Dr. Hiroshi Shimizu and Dr. Akihiko Shibaki, Department of Dermatology, Hokkaido University Graduate School of Medicine, N.15 W.7, Kita-ku, Sapporo 060-8638, Japan. E-mail addresses: shimizu@med.hokudai.ac.jp or ashibaki@med.hokudai.ac.jp

Abbreviations used in this paper: BP, bullous pemphigoid; COL17, type XVII collagen; CsA, cyclosporin A; DEJ, dermal–epidermal junction; hCOL17, human COL17; hNC16A, human COL17 noncollagenous 16A domain; IF, immunofluorescence; LD, lamina densa; Tg, transgenic; Treg, regulatory T cell; WT, wild-type.

www.jimmunol.org/cgi/doi/10.4049/jimmunol.0903101

Immunization of mice by hCOL17*-transgenic skin grafting*

Immunization of the mice by *hCOL17*-transgenic (Tg) skin graft was performed according to the method reported by Olasz et al. (11). Briefly, full-thickness 1-cm^2 pieces of dorsal skin were removed from sacrificed *hCOL17*-Tg mice (*COL17*$^{m+/+,h+}$) and grafted onto the backs of gender-matched 6-wk-old C57BL/6 wild-type (WT) mice. After topical application of antibiotic ointment, the grafted site was covered with gauze and an elastic bandage for 14 d. In selected experiments, WT mouse skin was grafted onto the backs of WT mice. Ab production was confirmed at 5 wk after skin grafting by indirect immunofluorescence (IF) analysis, as described below.

IF analysis

Indirect IF using mice sera was performed on the skin samples from human, COL17-humanized mice, or WT mice using standard protocols (1). In selected experiments, indirect IF was performed on 1 M NaCl-split normal human skin. We used FITC-conjugated Abs against mouse IgG (Jackson ImmunoResearch Laboratories, West Grove, PA), mouse IgG1, IgG2a, IgG2b, and IgG3 (BD Pharmingen, San Diego, CA), and mouse IgG2c (Bethyl Laboratories, Montgomery, TX) as the secondary Abs.

ELISA

To determine the Ab titer against hCOL17 noncollagenous 16A domain (hNC16A) in the serum samples from the experimental mice, 96-well microtiter plates coated with recombinant hNC16A protein purchased from Medical & Biological Laboratories (Nagoya, Japan) were incubated with diluted mouse sera for 1 h at room temperature. After being washed, bound Abs were developed with a 40,000-fold–diluted, HRP-labeled Ab specific to mouse IgG (Jackson ImmunoResearch Laboratories), and the OD was read at 450 nm using an ELISA plate reader (Mithras; Berthold Technologies, Bad Wildbad, Germany). The ELISA index value was defined by the following formula: index = (OD_{450} of tested serum − OD_{450} of negative control)/(OD_{450} of positive control − OD_{450} of negative control) × 100 (10).

Immunoblotting

Immunoblotting was performed as described previously (1). Recombinant proteins were subjected to SDS-PAGE and electrotransferred onto nitrocellulose membrane (Trans-Blot; Bio-Rad, Hercules, CA). The membranes were blocked and incubated at room temperature for 1 h with diluted sera obtained from experimental mice. After being washed, the membranes were incubated with alkaline phosphatase-conjugated anti-mouse IgG (Zymed Laboratories, South San Francisco, CA). The bound Abs were detected by the Western Blue Stabilized Substrate for Alkaline Phosphatase (Promega, Madison, WI).

Complement fixation study

Complement activation induced by Abs obtained from the immunized WT mice against the COL17 in human skin samples was investigated by IF microscopy as previously described, with minor modifications (12). Cryosections of human skin were incubated with IgG (10 μg/ml) from immunized WT mice for 1 h at 37°C. Freshly prepared mouse serum was then added as a complement source. One hour after incubation, in situ deposition of mouse complement C3 was detected with FITC-conjugated Abs specific to mouse C3 (Cappel; Valeant Pharmaceuticals, Costa Mesa, CA).

Adoptive transfer of splenocytes

Splenocytes were isolated and pooled from several immunized WT mice at 35 d after the skin grafting and administered to *Rag-2*$^{-/-}$/COL17–humanized or *Rag-2*$^{-/-}$ mice by i.v. injection into the tail vein with 2.0 × 10^8 splenocytes in 500 μl PBS per mouse (10).

ELISPOT assay

ELISPOT assay was performed as previously described (10, 13) with some minor modifications. Polyvinylidene difluoride-bottomed 96-well multiscreen plates (Millipore, Bedford, MA) were coated with 30 μg/ml recombinant hNC16A protein. In some experiments, 30 μg/ml recombinant mouse noncollagenous 14A domain protein was coated as negative controls. Mononuclear cells isolated from the spleen, bone marrow, and lymph nodes of the *Rag-2*$^{-/-}$/COL17–humanized recipients were incubated on the plate at 37°C in a 5% CO_2 incubator for 4 h. IgG bound to the membrane was visualized as spots with alkaline phosphatase-conjugated anti-mouse IgG Abs. The number of spots was counted under a dissecting microscope (SMZ1500; Nikon, Tokyo, Japan), and the frequency of anti-hNC16A IgG-producing B cells was defined as the number of spots in 10^5 mononuclear cells.

Evaluation of recipient mice

Weekly, the recipient mice were examined for their general condition and cutaneous lesions (i.e., erythema, hair loss, blisters, erosions, and crusts). Extent of skin disease was scored as follows: 0, no lesions; 1, lesions on <10% of the skin surface; 2, lesions on 10–20% of the skin surface; 3, lesions on 20–40% of the skin surface; 4, lesions on 40–60% of the skin surface; 5, lesions on >60% of the skin surface, as previously described (14) with minor modifications. Serum samples were also obtained from recipient mice weekly and assayed by indirect IF microscopy and hNC16A ELISA. Biopsies of lesional and perilesional skin were obtained between 2 and 5 wk after adoptive transfer for light microscopy (H&E), for toluidine blue staining to evaluate mast cell infiltration and degranulation, and for direct IF using FITC-conjugated Abs against mouse IgG, IgG1, IgG2a, IgG2b, IgG2c, IgG3, and C3.

Immunoelectron microscopy

Postembedding immunoelectron microscopy of cryofixed and cryosubstituted skin samples taken from the *Rag-2*$^{-/-}$/COL17–humanized mice at 5 wk after the adoptive transfer of immunized splenocytes was performed as previously described (15, 16) with minor modifications. Small pieces of fresh skin were cryofixed by plunging them into liquid propane at −190°C using a freeze–plunge apparatus (Leica Microsystems, Cambridge, U.K.). Skin samples were then cryosubstituted with methanol at −80°C using an automated freeze substitution system (Leica Microsystems) and embedded in Lowicryl K11M (Ladd Research Industries, Williston, VT) at −60°C. Ultrathin sections were incubated with 5-nm gold-labeled goat anti-mouse IgG (Biocell Laboratories, Rancho Dominguez, CA) and observed with a transmission electron microscope (H-7100; Hitachi High-Technologies, Tokyo, Japan).

Preparation of IgG fractions from mice and passive-transfer studies

Sera were obtained from *Rag-2*$^{-/-}$/COL17–humanized mice at 8 d after the adoptive transfer of immunized splenocytes. Total IgG was prepared from the sera by affinity chromatography using a HiTrap Protein G HP (GE Healthcare Biosciences, Uppsala, Sweden). We performed passive transfer of IgG into mice as previously described (1). A 60-μl dose of sterile IgG in PBS was administered to neonatal COL17-humanized mice by i.p. injection (0.1, 0.5, or 1.0 mg/g body weight). As a control, we prepared the total IgG fractions from WT mice and i.p. injected them into neonatal COL17-humanized mice (1.0 mg/g body weight). We judged skin phenotype at 48 h after the injection. The animals were then sacrificed, and skin sections were taken for histological examination.

Depletion of CD4$^+$ *or CD8*$^+$ *T cells or CD45R*$^+$ *B cells from immunized splenocytes*

For adoptive transfer of immunized splenocytes without $CD4^+$ or $CD8^+$ T cells or $CD45R^+$ B cells, we depleted each fraction from splenocytes of the immunized WT mice by using microbeads conjugated to monoclonal anti-mouse CD4 (L3T4), anti-mouse CD8a (Ly-2), or anti-mouse CD45R (B220) Abs (Miltenyi Biotec, Auburn, CA). The depletions of $CD4^+$ or $CD8^+$ T cells or $CD45R^+$ B cells were confirmed by flow cytometric analysis on a FACSAria (BD Pharmingen) as described below. Approximately 1.0 to 2.0 × 10^8 splenocytes depleted with $CD4^+$ or $CD8^+$ T cells or $CD45R^+$ B cells were adoptively transferred to *Rag-2*$^{-/-}$/COL17–humanized mice.

Administration of cyclosporin A to the BP model mice

Cyclosporin A (CsA) (Novartis Pharma, Basel, Switzerland) dissolved in olive oil was given i.p. at the dose of 35 mg/kg (100 μl) from 2 d after the adoptive transfer and continued daily for 14 d. The dose was chosen based on a previous study (17) and our preliminary data. As a control, the same volume of olive oil was injected into the BP model mice. The treated BP model mice were observed for 5 wk to evaluate the efficacy of the treatments.

Flow cytometry

The following mAbs were purchased from BD Pharmingen: 145-2C11-FITC (anti-CD3ε), H129.19-FITC (anti-CD4), 53-6.7-PE (anti-CD8), and RA3-6B2-PE (anti-CD45R/B220). One million cells were stained and subjected to analysis using a FACSAria.

Statistical analysis

To compare ELISA index values of Abs, the weights of mice, and the numbers of splenocytes, Student *t* tests were applied. We determined the statistical differences between groups of indirect IF titer and disease severity using the

Mann-Whitney U test or ANOVA with the Scheffe F test. Data were expressed as mean ± SE. We considered p values of <0.05 as significant.

Results

High titer of anti-hCOL17 IgG is induced in WT mice by hCOL17-Tg skin graft immunization

To induce anti-hCOL17 IgG Abs, WT mice were immunized by skin grafting from *hCOL17*-Tg mice, which express hCOL17 in the epidermis under the control of the human keratin 14 promoter (1, 11, 18). As reported by Olasz et al. (11), a high titer of IgG Abs specific to hNC16A was produced within 5 wk after the skin grafting. Levels of IgG Abs specific to hNC16A were measured by ELISA. The ELISA index values of sera from WT mice immunized by *hCOL17*-Tg skin grafting showed significantly higher reactivity than those values of sera from control WT skin-grafted WT mice (74.9 ± 13.5 versus 1.5 ± 1.0, $p < 0.01$) (Fig. 1*A*). Immune serum was analyzed by indirect IF, which revealed the deposition of IgG Abs at the dermal–epidermal junction (DEJ) of COL17-humanized mouse skin (Fig. 1*B*). There was no reactivity against WT mouse skin (Fig. 1*C*). We prepared the IgG fractions of sera from WT mice immunized by COL17-Tg skin grafting by affinity chromatography and determined the complement-fixing activity of purified IgG by indirect IF analysis. We found that 10 μg purified IgG could fix mouse C3 contained in freshly prepared mouse serum to the DEJ of normal human skin, whereas mouse C3 without purified IgG could not bind to the DEJ (Fig. 1*D*, 1*E*). The IgG subclass of anti-hCOL17 Abs present in the serum of each WT mouse immunized by *hCOL17*-Tg skin grafting was assessed by indirect IF analysis ($n = 10$). The deposition of IgG1, IgG2a, IgG2b, IgG2c, or IgG3 at the DEJ of normal human skin was observed in 100, 20, 10, 70, or 0% of the analyzed sera, respectively. Thus, immunized WT mice produce high titers of IgG1 and IgG2c anti-hCOL17 Abs that have complement-fixing activity.

Splenocytes transferred from the immunized mice produce a high titer of pathogenic anti-hCOL17 IgG Abs in the Rag-$2^{-/-}$/*COL17–humanized recipients*

To develop an active disease model for BP targeting humanized pathogenic Ag, we generated immunodeficient *Rag*-$2^{-/-}$/COL17–humanized (*Rag*-$2^{-/-}$/*COL17*$^{m-/-,h+}$) mice. First, we crossed COL17-humanized (*COL17*$^{m-/-,h+}$) mice with immunodeficient *Rag*-$2^{-/-}$ mice to generate *Rag*-$2^{+/-}$/*COL17*$^{m+/-,h+}$ mice. Next, those *Rag*-$2^{+/-}$/*COL17*$^{m+/-,h+}$ mice were crossed with each other, and the genotypes of the offspring were carefully screened. After four to five repeated crossings, we finally obtained the *Rag*-$2^{-/-}$/COL17–humanized mice. As a next step, splenocytes from some of the immunized WT mice were pooled after isolation and then adoptively transferred into the *Rag*-$2^{-/-}$/COL17–humanized mice that expressed hCOL17 protein in vivo ($n = 10$). Because these *Rag*-$2^{-/-}$/COL17–humanized mice had no mature T or B cells, they were able to accept the transferred splenocytes. All of the *Rag*-$2^{-/-}$/COL17–humanized recipients that were given immunized splenocytes produced IgG Abs against hCOL17 (Fig. 2*C*, 2*D*, Table I). Indirect IF examination revealed that IgG Abs produced in the recipients bound to the DEJ of normal human skin and COL17-humanized mouse skin but not to WT mouse skin. IF analysis using 1 M NaCl-split normal human skin as a substrate showed linear deposition of IgG on the epidermal side (Fig. 2*A*). Immunoblot analysis revealed that the recipients' sera reacted with both recombinant hCOL17 and hNC16A (Fig. 2*B*). Time-course analysis revealed that anti-DEJ IgG, which reflects the presence of anti-hCOL17 IgG, became detectable in recipients' sera within 1 wk after the transfer and that the titer peaked around

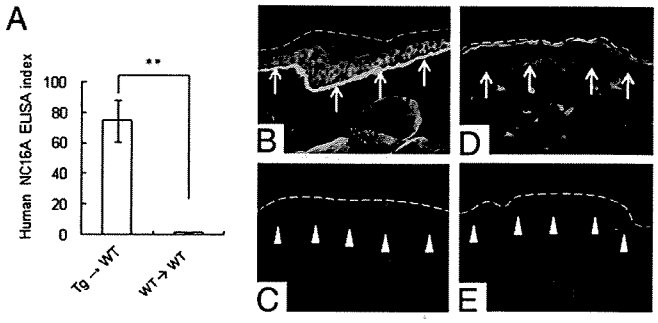

FIGURE 1. Circulating IgG Abs in the WT mice immunized by *hCOL17*-Tg skin grafting (immunized WT mice) recognize recombinant hNC16A and the DEJ of COL17-humanized mouse skin and activate mouse complement C3 in vitro. *A*, Anti-hNC16A IgG Abs are measured by ELISA. The index values of sera from immunized WT mice (Tg → WT) demonstrate significantly higher reactivities than those of sera from WT mice grafted with WT skin (WT → WT). *B* and *C*, The sera from immunized WT mice show positive reaction at the DEJ of COL17-humanized mouse skin (arrows) (*B*) but no specific reaction in WT mouse skin (arrow heads) (*C*) by indirect IF microscopy (original magnification ×200). *D* and *E*, Purified IgG from the immunized WT mice is able to fix mouse C3 to the DEJ (arrows) (*D*); no significant complement fixation is observed without the purified IgG from the immunized WT mice (arrow heads) (*E*). FITC-conjugated anti-mouse C3 Ab is used for the analysis (original magnification ×200). $^{**}p < 0.01$

day 9 after the transfer. Although the titer gradually decreased after the peak, it remained high (>5120×) for >10 wk without boosting (Fig. 2*C*). ELISA analysis revealed that anti-hNC16A IgG Abs appeared in the recipients' sera as early as 1 wk after the transfer. The Ab level rapidly increased, peaking around day 9 after the transfer. Although the titer gradually decreased, falling to a stable level at 6 wk after the transfer, anti-hNC16A IgG Abs were detectable for >10 wk without boosting (Fig. 2*D*). These results demonstrate that splenocytes from immunized WT mice can survive in the *Rag*-$2^{-/-}$/COL17–humanized recipients and produce a high titer of anti-hCOL17 Abs containing IgG against hNC16A. ELISPOT assay revealed that anti-hNC16A IgG-producing B cells in the *Rag*-$2^{-/-}$/COL17–humanized recipients existed mainly in the spleen and lymph nodes but not in bone marrow at days 9 and 10. Although the number of anti-hNC16A IgG-producing B cells decreased at day 52, it still remained detectable (Table II).

As a control, immunized splenocytes were also transferred into *Rag*-$2^{-/-}$ mice ($n = 6$). Interestingly, neither anti-DEJ nor anti-hNC16A IgG Abs were detected in control *Rag*-$2^{-/-}$ recipients (Fig. 2*C*, 2*D*, Table I). To exclude the possibility that transferred splenocytes cannot survive in the *Rag*-$2^{-/-}$ recipients, we grafted *hCOL17*-Tg skin onto the *Rag*-$2^{-/-}$ recipients 5 wk after the adoptive transfer of immunized splenocytes ($n = 3$). A high titer of anti-hCOL17 IgG Abs was detected within 14 d after the skin grafting in the *Rag*-$2^{-/-}$ recipients (data not shown). These results demonstrate that splenocytes transferred from the immunized WT mice can produce a high titer of anti-hCOL17 IgG Abs in the *Rag*-$2^{-/-}$/COL17–humanized recipients but not in the *Rag*-$2^{-/-}$ recipients.

Rag-$2^{-/-}$*/COL17–humanized mice given immunized splenocytes develop the BP phenotype*

The phenotypes observed in the recipient mice are summarized in Table I. Around day 7 after the adoptive transfer, the *Rag*-$2^{-/-}$/5COL17–humanized recipients began to scratch their snouts, muzzles, ears, and chests. Patchy hair loss associated with erythema began to develop on the chest between 9 and 14 d after the

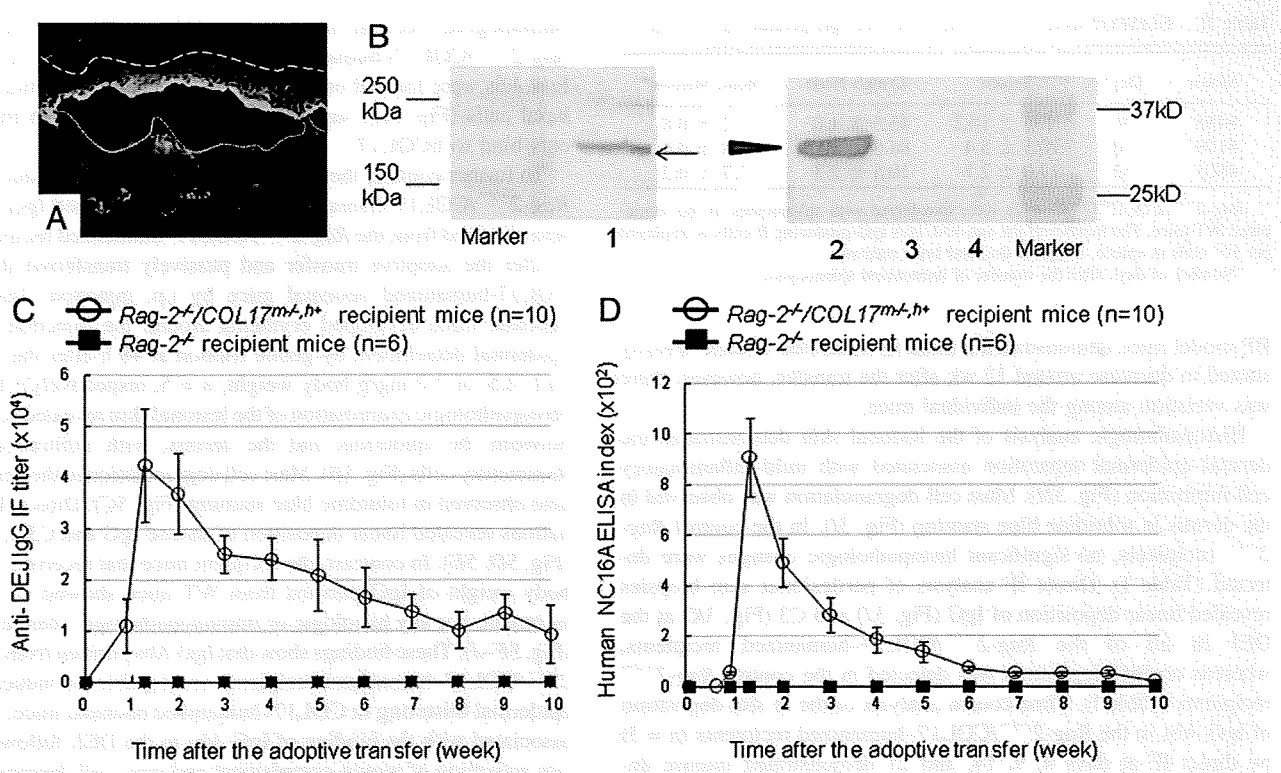

FIGURE 2. *Rag-2*$^{-/-}$/COL17–humanized mice given immunized splenocytes produce anti-hCOL17 Abs in vivo. *A*, Sera from the *Rag-2*$^{-/-}$/COL17–humanized recipients react to the epidermal side of 1 M NaCl-split normal human skin in indirect IF microscopy (original magnification ×200). *B*, IgG purified from a *Rag-2*$^{-/-}$/COL17–humanized recipient serum binds to 180-kDa recombinant hCOL17 (*lane* 1) and 35-kDa recombinant hNC16A proteins (*lane* 2) but fails to bind to recombinant mouse noncollagenous 14A domain, corresponding to hNC16A (*lane* 3) or GST proteins (*lane* 4). *C*, Persistent production of anti-DEJ IgG Abs in the *Rag-2*$^{-/-}$/COL17–humanized recipients is detected by indirect IF analysis. The titers rapidly increase and peak around day 9 after the transfer, and then they gradually decrease. In contrast, no anti-DEJ IgG Abs are detected in control *Rag-2*$^{-/-}$ recipients (n = 10; controls, n = 6). *D*, The IgG titers of sera from the *Rag-2*$^{-/-}$/COL17–humanized recipients and control *Rag-2*$^{-/-}$ recipients were measured by recombinant hNC16A ELISA. The titers rapidly increased after the transfer, peak around 1 wk, and then gradually decrease, stabilizing at a low level 6 wk after the transfer. No anti-hNC16A IgG Abs are observed in control *Rag-2*$^{-/-}$ recipients (n = 10; controls, n = 6).

adoptive transfer in most of the recipients. Then, blisters and erosions spontaneously developed in the dehaired areas on the trunk (Fig. 3*A*). Genital erosions and ears swelling with crusts were also observed (Fig. 3*B*, 3*C*). The dehaired patches gradually enlarged and spread to other regions on the trunk over the next 2–4 wk, resulting in large areas of alopecia (Fig. 3*D*, 3*E*). The epidermis on the trunk and tail easily detached from the dermis by gentle friction (Fig. 3*F*, 3*G*). Disease severity, scored by the percentage of skin surface with the BP phenotype (14), plateaued 5 wk after the transfer (Fig. 4). Conversely, none of the control *Rag-2*$^{-/-}$ recipients developed any skin lesions (Fig. 4). Also, splenocytes from untreated WT mice produced very low levels of anti-hCOL17 and anti-hNC16A IgG Abs and failed to induce any phenotypic changes in the *Rag-2*$^{-/-}$/COL17–humanized recipients (data not shown). In addition, 3 out of 10 *Rag-2*$^{-/-}$/COL17–humanized recipients showed changes on <20% of the skin surface (Table I). In one of those three recipients, the index value of the hNC16A ELISA at day 9 was far lower than the average (85.3 versus 907.8), whereas the anti-hCOL17 IgG titer at day 9 checked by indirect IF analysis was similar to the average. The other two recipients with changes of <20% of the surface showed no obvious difference in the IgG titers compared with the average. Long-term follow-up of

Table I. *Summary of phenotypes observed in recipient mice*

Donor	Recipient	n	Serum Abs		Subepidermal Separation in H&E Staining	Mast Cell Degranulation in Toluidine Blue Staining	Skin Immunopathology[c]		Skin Changes[d]
			IF[a]	ELISA[b]			IgG	C3	
C57BL/6 immunized by Tg[e] skin grafting	*Rag-2*$^{-/-}$/*COL17*$^{m-/-,h+}$	10	10/10	10/10	8/10	10/10	10/10	10/10	7/10
C57BL/6 immunized by Tg[e] skin grafting	*Rag-2*$^{-/-}$	6	0/6	0/6	0/6	0/6	0/6	0/6	0/6

[a]Linear deposition of IgG at the DEJ of the skin was detected by indirect IF microscopy on normal human skin cryosections using 40-fold–diluted recipient mouse serum obtained 2 wk after the adoptive transfer of splenocytes.

[b]Circulating IgG was tested with ELISA against recombinant hNC16A protein using 300-fold–diluted mouse serum obtained 2 wk after the adoptive transfer. The cutoff index value was set at 20.

[c]In vivo IgG and complement C3 deposition at the DEJ of the skin was determined by direct IF of perilesional skin biopsies. Medium or intense staining was regarded as positive.

[d]Skin changes including erythema, hair loss, bullae, and erosions exceeding 20% of the skin surface were considered significant.

[e]Tg: *hCOL17*-transgenic. The recipients in this table are those shown in Figs. 2*C*, 2*D*, and 4.

Table II. *ELISPOT assay of the anti-hNC16A IgG-producing B cells*

Mouse	Day[a]	Spleen	Lymph Node	Bone Marrow
#488	9	135 ± 16.2	43.5 ± 4.0	2 ± 0.8
#109	10	70.5 ± 5.4	84.0 ± 10.5	3.8 ± 0.6
#805	52	17.0 ± 2.7	10.5 ± 2.3	1.7 ± 0.2

Rag-2$^{-/-}$*/COL17*$^{m-/-,h+}$ mice were transferred with splenocytes of the immunized WT mice. The number of the anti-hNC16A IgG-producing B cells is displayed per 10^5 cells in spleen, lymph nodes, and bone marrow.

[a]Number of days after the transfer of immunized splenocytes.

BP model mice demonstrated a trend in which the disease severity started to decrease around 12 wk after the transfer; however, there was variation among the individual mice.

Histopathologic analysis of the lesional skin demonstrated the dermal–epidermal separation associated with mild inflammatory cell infiltration (Fig. 3*H*). Mast cell degranulation was observed in the dermis in toluidine blue staining (Fig. 3*I*). In the control *Rag-2*$^{-/-}$ recipients, no significant histopathologic changes were detected (Table I). Direct IF analysis of perilesional skin biopsies revealed linear deposition of IgG (Fig. 3*J*) and C3 (Fig. 3*K*) at the DEJ in all of the *Rag-2*$^{-/-}$/COL17–humanized recipients, whereas no IgG deposition was detected in the control *Rag-2*$^{-/-}$ recipients (Table I). Time-course analysis of the in situ deposition of IgG Abs in the *Rag-2*$^{-/-}$/COL17–humanized recipients ($n = 3$) by direct IF at days 4, 9, 14, and 21 demonstrated intense deposition of anti-hCOL17 IgG Abs at the DEJ as early as day 9 after the adoptive transfer, and the same levels of deposition were observed at days 14 and 21.

The subclasses of IgG produced in the *Rag-2*$^{-/-}$/COL17–humanized recipients were also analyzed by direct IF ($n = 10$). All of the *Rag-2*$^{-/-}$/COL17–humanized recipients showed a positive reaction with IgG1, IgG2a, IgG2b, and IgG2c Abs at the DEJ. Immunogold electron microscopy of the perilesional skin in the *Rag-2*$^{-/-}$/COL17–humanized recipients showed that anti-mouse IgG Abs were located on and around the plasma membrane of the basal cells (Fig. 3*L*), suggesting that Abs produced in the recipients bind to hCOL17.

To further confirm the pathogenicity of IgG Abs produced in the *Rag-2*$^{-/-}$/COL17–humanized recipients, we purified IgG from the sera obtained from the *Rag-2*$^{-/-}$/COL17–humanized recipients at 8 d after the adoptive transfer and passively transferred them into COL17-humanized neonatal mice by i.p. injection. Transferred neonatal mice developed erythema around the injection site and epidermal detachment by gentle friction at 48 h after the injection (0.1, 0.5, or 1.0 mg/g body weight, $n = 5$, respectively) (Fig. 5*A*). Histopathologic examination of the lesional skin revealed separation between the epidermis and the dermis, with infiltration of inflammatory cells (Fig. 5*B*). Mast cell degranulation in the dermis was also observed in toluidine blue staining (Fig. 5*C*). Direct IF examinations revealed linear deposition of mouse IgG and C3 at the DEJ (Fig. 5*D*, 5*E*). In contrast, the recipient mice that received 1.0 mg/g body weight of IgG purified from WT mice showed no skin detachment, nor any histologic or immunopathologic changes ($n = 5$) (Fig. 5*F–J*). These findings show that IgG Abs purified from the *Rag-2*$^{-/-}$/COL17–humanized recipients are capable of inducing subepidermal blistering in COL17–humanized neonatal mice, which is associated with the binding of IgG Abs to the DEJ, followed by in situ activation of mouse complement and mast cell degranulation.

CD4$^+$ *T cells as well as CD45R*$^+$ *B cells are essential for the stable production of anti-hCOL17 IgG Abs in the* Rag-2$^{-/-}$*/COL17–humanized recipients*

To determine the pathogenic roles of T cells and B cells in the *Rag-2*$^{-/-}$/COL17–humanized recipients, we depleted CD4$^+$ or CD8$^+$ T cells or CD45R$^+$ B cells from splenocytes of the immunized WT

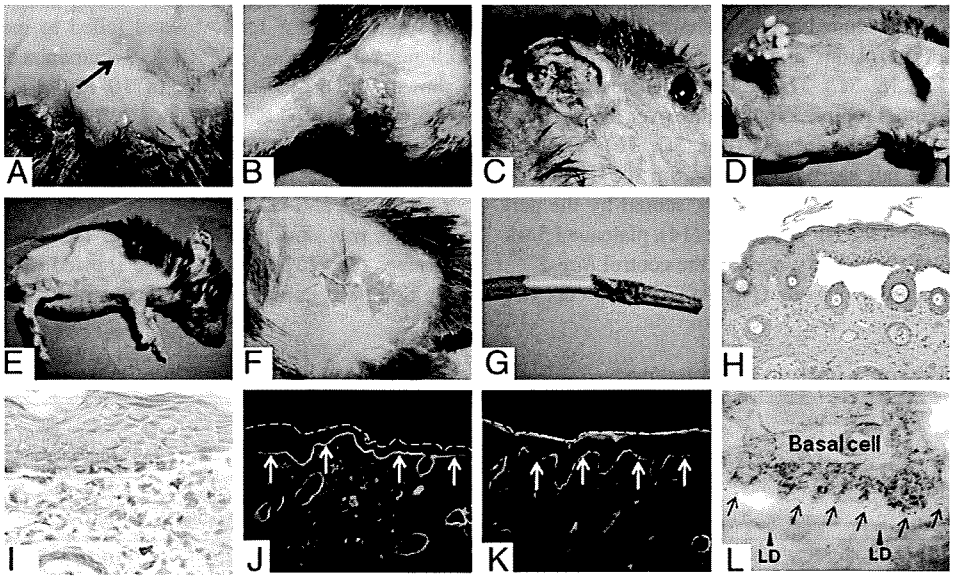

FIGURE 3. *Rag-2*$^{-/-}$/COL17–humanized mice given immunized splenocytes demonstrate the BP phenotype associated with histologic and immunopathologic changes similar to BP. *A*, Spontaneously developing blisters are observed in the *Rag-2*$^{-/-}$/COL17–humanized recipients 3 wk after the transfer (arrow). *B* and *C*, Genital erosions and ear swelling with crusts are seen in the recipients. *D* and *E*, Large, diffuse patches of hair loss associated with erythema, erosions, and crusts on the trunk and the paws. *F* and *G*, Epidermal detachment by gentle friction on the trunk and tail is characteristically observed. *H*, Histologic examination of diseased mice reveals separation between dermis and epidermis with mild inflammatory cell infiltration in H&E staining (original magnification ×200). *I*, Mast cell degranulation in the dermis is observed in toluidine blue staining (original magnification×400). *J* and *K*, Direct IF analysis of lesional skin biopsy reveals linear deposition of mouse IgG (arrows) (*J*) and mouse C3 (arrows) (*K*) along the DEJ (original magnification ×200). *L*, Immunoelectron microscopy demonstrates that mouse IgG Abs deposit at the DEJ close to the plasma membranes of basal cells in the skin of the *Rag-2*$^{-/-}$/COL17–humanized recipient (arrows). LD, lamina densa.

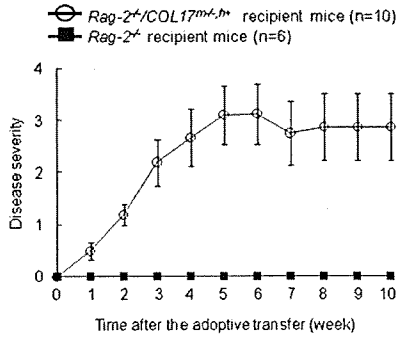

FIGURE 4. *Rag-2*$^{-/-}$/COL17–humanized mice given immunized splenocytes develop the BP disease phenotype. Disease severities of the *Rag-2*$^{-/-}$/COL17–humanized recipients gradually increase, plateauing 5 wk after the transfer. None of the control *Rag-2*$^{-/-}$ recipients develop any skin lesions (n = 10; controls, n = 6). Disease severity is scored as described in *Materials and Methods*.

mice and adoptively transferred them into the *Rag-2*$^{-/-}$/COL17–humanized mice. All of the recipient mice given immunized splenocytes after the depletion of CD8$^+$ T cells produced a high titer of anti-hCOL17 IgG Abs and developed severe BP lesions associated with histopathologic and immunopathologic changes indistinguishable from those of the *Rag-2*$^{-/-}$/COL17–humanized mice given whole immunized splenocytes (n = 4) (Fig. 6). In contrast, the depletion of CD4$^+$ T cells or CD45R$^+$ B cells inhibited the production of anti-hCOL17 IgG Abs and the development of the BP phenotype (n = 4, respectively) (Fig. 6). These findings indicate that CD4$^+$, but not CD8$^+$, T cells and CD45R$^+$ B cells are crucial for the production of anti-hCOL17 IgG Abs and for the development of the BP phenotype.

To further investigate the pathogenic role of CD4$^+$ T cells in the *Rag-2*$^{-/-}$/COL17–humanized recipients, we examined the efficacy of CsA (19–22). Approximately 35 mg/kg of CsA dissolved in olive oil (n = 5) or a control vehicle (n = 5) was i.p. injected into the *Rag-2*$^{-/-}$/COL17–humanized recipients from 2 d after the adoptive transfer of whole immunized splenocytes, once daily for 14 d. When the numbers of splenocytes at day 9 after the transfer were compared, the mean number of splenocytes in both groups was not significantly different (8.3×10^7 cells in the CsA-treated mice versus 11.0×10^7 cells in the control mice, $p > 0.05$). Although the mean percentage of CD3$^+$ T cells was significantly lower in the CsA-treated mice than that in the control mice (14.1% in the CsA-treated mice versus 24.5% in the control mice, $p < 0.05$), the mean percentages of CD45R$^+$ B cells were similar in both groups (28.8% in the CsA-treated mice versus 26.5% in the control mice, $p > 0.05$). Disease severity and the titers of circulating anti-hNC16A IgG Abs were significantly lower in the treated mice than those in the controls (Fig. 7). This result further suggests that CD4$^+$ T cells play a pivotal role in the pathogenesis of this BP model.

Discussion

This is the first active BP model that stably produces pathogenic anti-hCOL17 Abs and spontaneously develops blisters and erosions on the skin. Because amino acid sequences of COL17, especially those of the noncollagenous 16A domain region, are different between human and mouse, an animal model using COL17-humanized mice that express hCOL17 is suitable for analyzing pathogenic mechanisms of human BP. Therefore, we developed an active BP model in which the targeted pathogenic Ag is hCOL17 but not mouse COL17. Immunized splenocytes transferred into immunodeficient *Rag-2*$^{-/-}$/COL17–humanized recipients survived and continuously produced a high titer of anti-hCOL17 Abs in vivo for >10 wk after the adoptive transfer. Those Abs bound to the hCOL17 molecules that were expressed in the recipients' skin, which initiated subsequent immune reactions including complement activation and mast cell degranulation, resulting in dermal–epidermal separation. This array of immune responses was consistent with the pathogenic mechanisms of BP previously demonstrated in passive-transfer neonatal mouse models (1, 12, 23–25). Furthermore, the *Rag-2*$^{-/-}$/COL17–humanized recipients developed blisters and erosions on erythematous skin areas that lasted >10 wk. The pathogenicity of anti-hCOL17 IgG Abs was confirmed by passive-transfer experiments that revealed that IgG Abs obtained from the *Rag-2*$^{-/-}$/COL17–humanized recipients could induce the BP phenotype in COL17-humanized neonatal mice. Thus, pathogenic anti-hCOL17 IgG Abs produced in the *Rag-2*$^{-/-}$/COL17–humanized recipient binds to the target Ag in vivo and induces the BP phenotype. By using COL17-humanized mice, we can observe the dynamic immune reactions induced by pathogenic Abs against hCOL17 molecules. These strategies for the production of active autoimmune disease models targeting humanized pathogenic Ag can also be applied to other autoimmune diseases.

In BP, complement activation is considered to be critical for blister formation (26). The first evidence suggesting the pathogenic role of complements in BP is the demonstration of C3

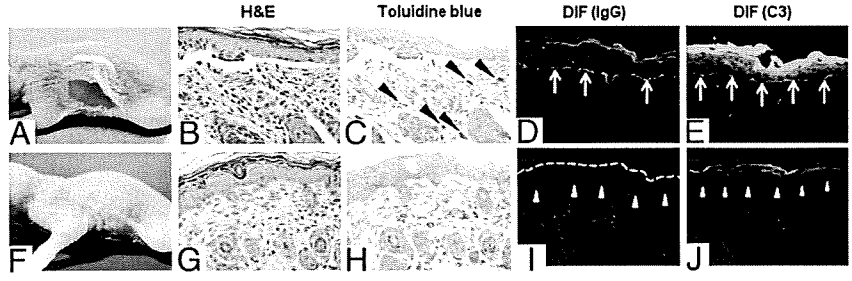

A-E: COL17-humanized mice injected with 1.0mg/g IgG from *Rag-2*$^{-/-}$/COL17-humanized recipient mice (Day 8)
F-J: COL17-humanized mice injected with 1.0mg/g IgG from Wt mice

FIGURE 5. COL17-humanized neonatal mice injected with IgG purified from the *Rag-2*$^{-/-}$/COL17–humanized recipients at 8 d after the adoptive transfer show skin fragility and histologic and immunopathologic changes similar to BP. *A*, The recipient mice develop epidermal detachment by gentle friction at 48 h after injection of the 1.0 mg/g IgG purified from the *Rag-2*$^{-/-}$/COL17–humanized recipients (n = 5). *B*, Histologic examination reveals subepidermal separation associated with mild inflammatory cell infiltrates in H&E staining (original magnification ×200). *C*, Mast cell degranulation in the dermis (arrow heads) is observed in toluidine blue staining (original magnification ×400). *D* and *E*, Direct IF studies show linear deposition of mouse IgG (arrows) (*D*) and C3 (arrows) (*E*) at the DEJ (original magnification ×200). *F–J*, No phenotypic or histological findings are observed in the mice injected with 1.0 mg/g IgG purified from sera of WT mice grafted with WT skin (n = 5).

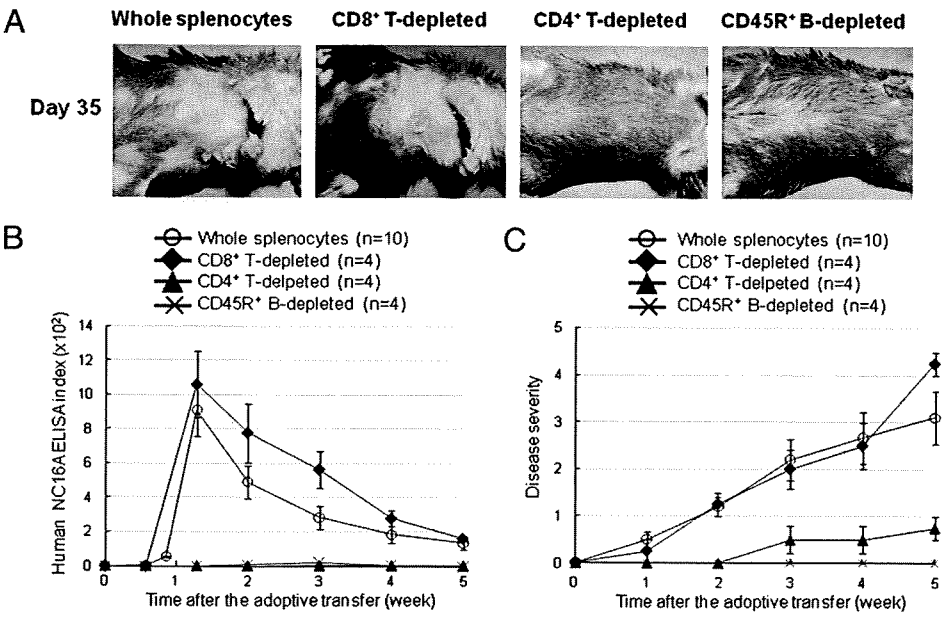

FIGURE 6. The production of anti-hCOL17 IgG Abs requires $CD4^+$ T cells and $CD45R^+$ B cells but not $CD8^+$ T cells. *A*, All of the recipients given $CD8^+$ T cell-depleted splenocytes (n = 4) develop severe BP lesions similar to those of the recipients given whole splenocytes, whereas the recipients given $CD4^+$ T cell-depleted splenocytes (n = 4) or $CD45R^+$ B cell-depleted splenocytes (n = 4) demonstrate no erosive lesions. *B*, The depletions of $CD4^+$ T cells or $CD45R^+$ B cells significantly inhibit the production of anti-hNC16A IgG Abs ($p < 0.01$ at day 9). *C*, The recipients given $CD4^+$ T cell-depleted or $CD45R^+$ B cell-depleted splenocytes show significantly lower disease severities than those in other groups ($p < 0.05$ at days 14 and 35).

deposition at the basement membrane zone of the lesional and perilesional skin by direct IF (27). By means of the passive-transfer experiments using C5-deficient mice, Liu et al. (25) further showed that complement activation is a pivotal step in subepidermal blister formation triggered by rabbit anti-mouse COL17 IgG Abs in their BP animal model. Consistent with these previous studies, linear deposition of complement C3 was observed at the DEJ in all of the diseased *Rag-2*$^{-/-}$/COL17–humanized recipients. We also demonstrated that sera from both the immunized WT mice and the *Rag-2*$^{-/-}$/COL17–humanized recipients contained complement-fixing Abs of the IgG2 subclass and could fix compliments at the DEJ of the normal human skin and the COL17-humanized skin. Analysis of the subclass distribution of IgG autoantibodies in human BP revealed that complement-fixing IgG1 was present as the predominant subclass of autoantibodies (28). These findings suggest that complement activation mediated by Abs of the IgG2 subclass against hCOL17 may induce blister formation in the present BP model.

It is unclear why the anti-hCOL17 IgG titer decreases in a short period. To examine the possible compartmentalization of anti-hCOL17 IgG response to the skin, we checked in situ deposition of anti-hCOL17 IgG in the skin of BP model mice by direct IF analysis sequentially at days 4, 9, 14, and 21. Intense deposition of anti-hCOL17 IgG Abs was detected at the DEJ as early as day 9 of the adoptive transfer, and the same levels of deposition were observed at days 14 and 21 (n = 3). This indicates that the compartmentalization of the anti-hCOL17 IgG response to the skin is not the main reason for the spontaneous reduction of the anti-hCOL17 IgG titer in this BP model. Alternatively, some regulatory mechanism against hCOL17-specific T cells, B cells, or both may be induced in this BP model. In experimental autoimmune myasthenia gravis, an autoimmune neuromuscular disease model induced by anti-acetylcholine receptor Abs, regulatory T cells (Tregs) generated ex vivo or expanded in vivo suppress pathogenic T cell and Ab responses (29, 30). In experimental autoimmune encephalomyelitis, a myelin-reactive T cell-dependent multiple

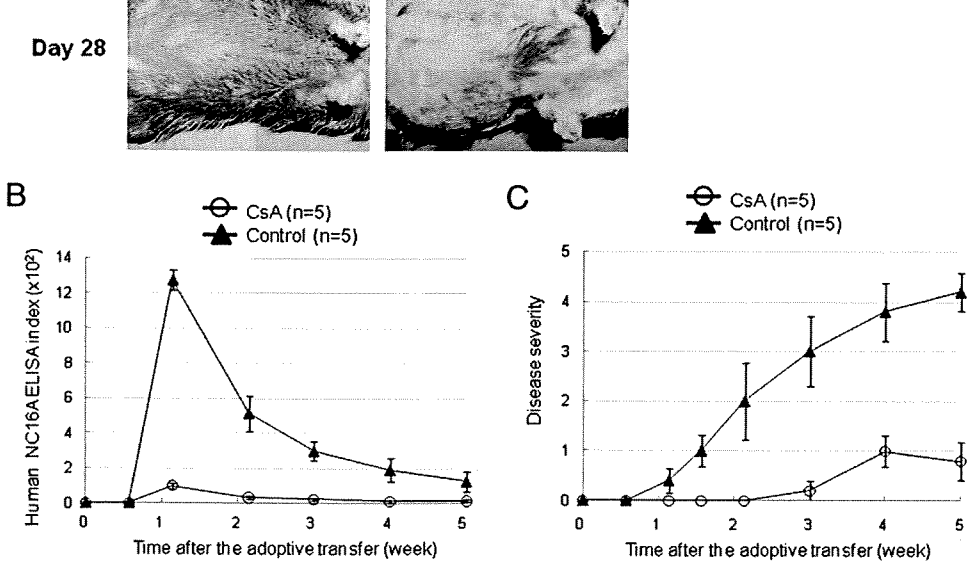

FIGURE 7. Results of CsA treatment in the *Rag-2*$^{-/-}$/COL17–humanized recipients. Approximately 35 mg/kg CsA was administered daily from 2 d after the adoptive transfer for 14 d (CsA, n = 5; control vehicle, n = 5). *A*, Skin lesions of the *Rag-2*$^{-/-}$/COL17–humanized recipients treated with CsA are markedly diminished with CsA treatment (day 28). *B*, CsA significantly suppresses the production of anti-hNC16A IgG ($p <$ 0.01 at days 8, 15, and 21). *C*, The treated mice show significantly lower disease severity than that of the controls ($p < 0.01$ at days 8, 15, 21, 28, and 35).

sclerosis model, natural resolution correlates with the accumulation of myelin-reactive Tregs expanded during the course of experimental autoimmune encephalomyelitis in the inflamed CNS (31, 32). Similar to these autoimmune disease models, Tregs may contribute to the spontaneous decline of the anti-hCOL17 IgG titer in this BP model. Further studies examining Treg function in this BP model may provide clues for controlling the autoimmune reaction in BP patients.

Interestingly, none of the control *Rag-2*$^{-/-}$ recipients given immunized splenocytes produced anti-hCOL17 IgG Abs or developed the BP phenotype despite the presence of living splenocytes in vivo. We further demonstrated that the grafting of *hCOL17*-Tg skin onto *Rag-2*$^{-/-}$ mice 5 wk after the adoptive transfer of immunized splenocytes could induce a high titer of anti-hCOL17 IgG Abs. These results indicate that transferred splenocytes need endogenous hCOL17 molecules to produce anti-hCOL17 IgG Abs. In addition, the depletion of CD4$^+$ T cells from the immunized WT splenocytes suppressed the production of anti-hCOL17 IgG Abs, whereas the depletion of CD8$^+$ T cells showed no effects. This clearly suggests that CD4$^+$ T cells, and not CD8$^+$ T cells, are essential for the production of Abs against hCOL17 in this BP model.

Generally, the production of Abs by B cells requires the help of CD4$^+$ T cells. In experimental autoimmune myasthenia gravis, both MHC class II gene-disrupted mice and CD4 gene knockout mice have been proven to be resistant to induction of clinical experimental autoimmune myasthenia gravis (33, 34). In experimental pemphigus vulgaris, an autoimmune blistering disease caused by anti-desmoglein 3 Abs, the production of autoantibodies required both CD4$^+$ T cells and B cells from naive desmoglein 3 knockout mice (35). To further investigate the pathogenic role of CD4$^+$ T cells, we administered CsA, an immunosuppressant that inhibits T cell function, to the *Rag-2*$^{-/-}$/COL17–humanized recipients after the adoptive transfer of immunized splenocytes. Because active disease models possess more persistent disease activity than passive-transfer neonatal disease models (10, 36, 37), we can easily analyze the time-course changes of disease activity altered by such an intervention. CsA significantly suppressed the production of anti-hNC16A IgG Abs and diminished the disease severity. These results strongly suggest that CD4$^+$ T cells play a pivotal role in the production of the autoantibodies through the presentation of the endogenous autoantigen. In human BP, the presence of autoreactive CD4$^+$ T cells has been reported, indicating the contribution of CD4$^+$ T cells to the pathogenesis of human BP (38–40). In addition, particular MHC class II alleles are more frequent in BP patients (41). These results further indicate that the autoreactive CD4$^+$ T cells may be activated through an interaction with the specific MHC class II molecule in BP. The pathogenic function of CD4$^+$ T cells shown in this BP model may provide a new insight into the pathogenic mechanism of BP and the development of a novel therapeutic strategy that targets T cell-mediated immune reactions.

Although this BP model is a useful tool for investigating the pathophysiology of BP, limitations are still present in our experimental system. First, the induction phase of the autoimmune response, such as the breakdown of self-tolerance, cannot be investigated in this BP model because the immune response to hCOL17 is induced by adoptive transfer of immunized WT splenocytes. To investigate the induction of autoimmunity in BP, Xu et al. (42) have aimed to induce autoimmune responses to mouse COL17 by using the immunocompetent BALB/c mice. Multiple immunizations of BALB/c mice with peptides of the hNC16A domain, its mouse equivalent, or both successfully induced anti-mouse COL17 IgG Abs, although no overt skin changes were observed. Similar experiments have been performed to establish an animal model for epidermolysis bullosa acquisita, a subepidermal blistering disorder induced by Abs against type VII collagen, another hemidesmosomal protein present at the basement membrane zone (43). Anti-type VII collagen Abs and subepidermal blisters were successfully induced in the mice by repeated immunizations with recombinant mouse type VII collagen protein mixed with adjuvant, although the development of the disease phenotype depended on the strain of mice. These results indicate that repeated exposure of the self Ag in conjunction with inflammatory stimulation, such as by bacterial components, may break down peripheral tolerance and induce autoantibody production in patients with a specific genetic background. This concept is further supported by the clinical findings that BP develops preferentially in elderly people and that particular HLA class II alleles correlate with BP patients (41). Second, this BP model demonstrates immune responses against a humanized Ag of the skin; however, the response still occurs in a murine milieu. The lack of eosinophilic infiltration, a characteristic trait of human BP, in this model could be related to the difference of the effector cell function between human and mouse immune systems. Furthermore, because the MHCs in mice are different from those in humans, MHC-dependent presentation of the pathogenic Ag to the T and B cells cannot be simulated in this current BP mouse model. To overcome these issues, not only the pathogenic Ag but also the immune system should be humanized in experimental animals. Recently, quasi-human immune systems have been stably reconstituted in supra-immunodeficient NOG mice using human CD34$^+$ stem cells from various sources including bone marrow, umbilical cord blood, and peripheral blood (44, 45). This system has become a common tool for studying human immunity and diseases relating to it (46, 47). However, even in that system the development of human B cells was partially blocked, and the human T cells lost their function in the periphery (48). Further technical advances would be required to establish more accurate and reliable humanized animal models that could be used toward better understanding human diseases that involve autoimmunity.

In summary, using immunodeficient COL17-humanized mice, we have successfully developed a novel active disease model for BP that continuously produces pathogenic anti-hCOL17 IgG Abs and reproduces the BP phenotype. This study indicates that a humanized animal model is quite valuable not only for analyzing biological function of human molecules but also for investigating pathogenic mechanisms of autoimmune diseases against human proteins. This new BP model can be used for the investigation of underlying mechanisms in the development and progression of BP. Furthermore, it should facilitate the development of novel therapeutic strategies for BP.

Acknowledgments

We thank Professor K. B. Yancey (Department of Dermatology, Medical College of Wisconsin, Milwaukee, WI) for providing the *COL17*$^{m+/+,h+}$ mice, Dr. K. Nishifuji and Professor M. Amagai (Department of Dermatology, Keio University School of Medicine, Tokyo, Japan) for their technical advice and valuable discussions on the ELISPOT assay, Dr. K. Iwabuchi (Division of Immunobiology, Institute for Genetic Medicine, Hokkaido University, Sapporo, Japan) for his valuable discussions, and Ms. N. Ikeda, Ms. Y. Kashima, Ms. M. Tanabe, and Ms. K. Sakai for their technical assistance.

Disclosures

The authors have no financial conflicts of interest.

References

1. Nishie, W., D. Sawamura, M. Goto, K. Ito, A. Shibaki, J. R. McMillan, K. Sakai, H. Nakamura, E. Olasz, K. B. Yancey, et al. 2007. Humanization of autoantigen. *Nat. Med.* 13: 378–383.